ISSN 2523-6881

Volume 7, Issue 19 – July – December – 2023

Journal Renewable Energy

ECORFAN®

Journal Renewable Energy, Volume 7, Issue 19, December 2023, is a journal edited six monthly by ECORFAN-Peru. 1047 La Raza Avenue -Santa Ana, Cusco-Peru. WEB: www.ecorfan.org/taiwan, revista@ecorfan.org. Chief Editor: SERRANO-PACHECO, Martha. PhD. ISSN-On line: 2523-6881. Responsible for the latest update of ECORFAN Computer Unit. ESCAMILLA-BOUCHÁN, Imelda, PhD, LUNA-SOTO, Vladimir. PhD. 1047 La Raza Avenue - Santa Ana, Cusco-Peru, last updated December 31, 2023.

Journal Renewable Energy

Definition of Research Journal

Scientific Objectives

Support the international scientific community in its written production Science, Technology and Innovation in the Field of Engineering and Technology, in Subdisciplines Solar energy and its applications, renewable energies and climate change, environmental impact, hydroelectric plants, renewable energies, energy geothermal power in the world.

ECORFAN-Mexico SC is a Scientific and Technological Company in contribution to the Human Resource training focused on the continuity in the critical analysis of International Research and is attached to CONAHCYT-RENIECYT number 1702902, its commitment is to disseminate research and contributions of the International Scientific Community, academic institutions, agencies and entities of the public and private sectors and contribute to the linking of researchers who carry out scientific activities, technological developments and training of specialized human resources with governments, companies and social organizations.

Encourage the interlocution of the International Scientific Community with other Study Centers in Mexico and abroad and promote a wide incorporation of academics, specialists and researchers to the publication in Science Structures of Autonomous Universities - State Public Universities - Federal IES - Polytechnic Universities - Technological Universities - Federal Technological Institutes - Normal Schools - Decentralized Technological Institutes - Intercultural Universities - S & T Councils - CONAHCYT Research Centers.

Scope, Coverage and Audience

Journal Renewable Energy is a Research Journal edited by ECORFAN-Mexico S.C in its Holding with repository in Republic of Peru, is a scientific publication arbitrated and indexed with semester periods. It supports a wide range of contents that are evaluated by academic peers by the Double-Blind method, around subjects related to the theory and practice of Solar energy and its applications, renewable energies and climate change, environmental impact, hydroelectric plants, renewable energies, energy geothermal power in the world with diverse approaches and perspectives , That contribute to the diffusion of the development of Science Technology and Innovation that allow the arguments related to the decision making and influence in the formulation of international policies in the Field of Engineering and Technology. The editorial horizon of ECORFAN-Mexico® extends beyond the academy and integrates other segments of research and analysis outside the scope, as long as they meet the requirements of rigorous argumentative and scientific, as well as addressing issues of general and current interest of the International Scientific Society.

Editorial Board

Arbitration Committee

Assignment of Rights

The sending of an Article to Journal Renewable Energy emanates the commitment of the author not to submit it simultaneously to the consideration of other series publications for it must complement the Originality Format for its Article.

The authors sign the Authorization Format for their Article to be disseminated by means that ECORFAN-Mexico, S.C. In its Holding Republic of Peru considers pertinent for disclosure and diffusion of its Article its Rights of Work.

Declaration of Authorship

Indicate the Name of Author and Coauthors at most in the participation of the Article and indicate in extensive the Institutional Affiliation indicating the Department.

Identify the Name of Author and Coauthors at most with the CVU Scholarship Number-PNPC or SNI-CONAHCYT- Indicating the Researcher Level and their Google Scholar Profile to verify their Citation Level and H index.

Identify the Name of Author and Coauthors at most in the Science and Technology Profiles widely accepted by the International Scientific Community ORC ID - Researcher ID Thomson - arXiv Author ID - PubMed Author ID - Open ID respectively.

Indicate the contact for correspondence to the Author (Mail and Telephone) and indicate the Researcher who contributes as the first Author of the Article.

Plagiarism Detection

All Articles will be tested by plagiarism software PLAGSCAN if a plagiarism level is detected Positive will not be sent to arbitration and will be rescinded of the reception of the Article notifying the Authors responsible, claiming that academic plagiarism is criminalized in the Penal Code.

Arbitration Process

All Articles will be evaluated by academic peers by the Double Blind method, the Arbitration Approval is a requirement for the Editorial Board to make a final decision that will be final in all cases. MARVID® is a derivative brand of ECORFAN® specialized in providing the expert evaluators all of them with Doctorate degree and distinction of International Researchers in the respective Councils of Science and Technology the counterpart of CONAHCYT for the chapters of America-Europe-Asia- Africa and Oceania. The identification of the authorship should only appear on a first removable page, in order to ensure that the Arbitration process is anonymous and covers the following stages: Identification of the Research Journal with its author occupation rate - Identification of Authors and Coauthors - Detection of plagiarism PLAGSCAN - Review of Formats of Authorization and Originality-Allocation to the Editorial Board- Allocation of the pair of Expert Arbitrators-Notification of Arbitration -Declaration of observations to the Author-Verification of Article Modified for Editing-Publication.

Instructions for Scientific, Technological and Innovation Publication

Knowledge Area

The works must be unpublished and refer to topics of Solar energy and its applications, renewable energies and climate change, environmental impact, hydroelectric plants, renewable energies, energy geothermal power in the world and other topics related to Engineering and Technology.

Presentation of the content

In the first article we present, *Quality analysis of electrical energy*, by NUÑEZ-GONZALEZ, Dioni Victoria, CARDONA-MARTINEZ, Clara, RODRIGUEZ-UGARTE, Maria Elena and GUEVARA-HERNANDEZ, Eduardo, with adscription in the Universidad Tecnológica de Querétaro, in the next article we present D*esign and construction of a solar simulator for characterization of photovoltaic modules*, by LÓPEZ-CARRILLO, José Luis, GARCÍA-PEDROZA, Luis Daniel, REYES-DURÁN, Bernardo and ÁLVAREZ-MACÍAS, Carlos, with adscription in the Tecnológico Nacional de México / Instituto Tecnológico de la Laguna, in the next article we present *Design considerations for the dimensioning of parabolic trough solar thermal plants*, by LIZÁRRAGA-MORAZÁN, Juan Ramón & PICÓN-NUÑEZ, Martin with adscription in the Universidad de Guanajuato, in the last article we present, *Geothermal energy harnessing using a horizontal composite geothermal heat exchanger and a vertical geothermal heat exchanger*, by RUBIO-LÓPEZ, Osvaldo, MONTOYA-SANTIYANES, Luis Alvaro, GARCÍA-GUENDULAIN, Juan Manuel and MENDOZA-ROJAS, América Eileen, with adscription in the Universidad Politécnica de Querétaro..

Content

Article **Journal Renewable Energy**
December, 2023 Vol.7 No.19 1-11

Quality analysis of electrical energy

Análisis de calidad de energía eléctrica

NUÑEZ-GONZALEZ, Dioni Victoria†, CARDONA-MARTINEZ, Clara*, RODRIGUEZ-UGARTE, Maria Elena and GUEVARA-HERNANDEZ, Eduardo

Universidad Tecnológica de Querétaro. División Tecnológica-Ambiental

ID 1st Author: *Dioni Victoria, Nuñez-Gonzalez* / **ORC ID**: 0009-0001-5545-1445, **CVU CONAHCYT ID**: 1302679

ID 1st Co-author: *Clara, Cardona-Martinez* / **ORC ID** 0000-0002-5241-020X, **CVU CONAHCYT ID**: 390947

ID 2nd Co-author: *Maria Elena, Rodriguez-Ugarte* / **ORC ID**: 0000-0002-0943-840X **CVU CONAHCYT ID**: 88108

ID 3rd Co-author: *Eduardo, Guevara-Hernandez* / **ORC ID**: 0000-0001-6209-2535, **CVU CONAHCYT ID**: 208765

DOI: 10.35429/JRE.2023.19.7.1.11 Received July 16, 2023; Accepted October 30, 2023

Abstract

This study exposes the measurements of electrical parameters carried out with a power quality analyzer in a transformer. The first measurement taking into account a capacitor bank that was already installed and then taking it out of operation. It presents the results graphed in "Power Log" and analyzed with respect to the standards CFE-L00045, IEEE 519-1992 and the Regulatory Manual of Technical Requirements for the Connection of Load Centers. By disconnecting the capacitor bank, with the data records obtained from the measurement, it is possible to consider adding a harmonic filter that is presented as the proposal for improving the quality of electrical power, since it achieves an increase from 0.73 to 0.98 in the power factor without compromising the permissible values of harmonics in the system. The filter is calculated and simulated in "DigSILENT Power Factory" to demonstrate the feasibility of the proposal.

Harmonics, Power Factor, Quality

Resumen

Este estudio expone las mediciones de parámetros eléctricos realizadas con un analizador de calidad de la energía en un transformador. La First Measurement tomando en cuenta un banco de capacitores que ya se encontraba instalado y después sacando este de la operación. Se presentan los resultados graficados en “Power Log” y analizados con respecto a las Regs CFE-L00045, IEEE 519-1992 y el Manual Regulatorio de Requerimiento Técnicos para la Conexión de Centros de Carga. Al desconectar el banco de capacitores, con los registros obtenidos de la medición, es posible considerar añadir un filtro de armónicos que se presenta como la propuesta para la mejora de calidad de energía eléctrica, ya que se logra un aumento de 0.73 a 0.98 en el factor de potencia sin comprometer los valores permisibles de armónicos en el sistema. El filtro es calculado y simulado en “DigSILENT Power Factory” para demostrar la factibilidad de la propuesta.

Armónicos, Factor de Potencia, Calidad

Citation: NUÑEZ-GONZALEZ, Dioni Victoria, CARDONA-MARTINEZ, Clara, RODRIGUEZ-UGARTE, Maria Elena and GUEVARA-HERNANDEZ, Eduardo. Quality analysis of electrical energy. Journal Renewable Energy. 2023. 7-19: 1-11

*Correspondence to Author (e-mail: ccardona@uteq.edu.mx)
† Researcher contributing as first author.

Introduction

The company specialized in the production of anti-refilling and aluminum closures has a focus on energy efficiency since most of its processes require electricity to function. The proposed aim for this project is to reduce the harmonics, concurrently increasing the power factor, which can interpret as a considerable reduction of the negative ecological impact and a financial improvement for the company.

In order to reduce the consumption of electrical energy, it has been proposed, to measure the electrical parameters and, based on the results obtained, propose the integration of a new component in the system, which will reduce the total cost of electrical energy consumed, and will have a trend close to the permissible values for the power factor which is one of the technical requirements applicable to consumer users in the IEEE 519-1992, CFE-L00045 and the Regulatory Manual of Technical Requirements for Center Connection of Load.

Background

The company specialized in the production of anti-refilling and aluminum closures has presented a power factor of 0.94pf. This parameter is an indicator on the utilization of energy, showing the relationship between the apparent power and the active power, the first being the required or demanded energy and the second, the energy that is really useful for the process. Despite the fact that the initially measured value of the power factor in the company is not low, it is not within the limits allowed by the Regulatory Manual of Technical Requirements for the Connection of Load Centers issued by the Energy Regulatory Commission, which indicates that this must be higher than or equal to 0.95pf (CRE, 2019). Failure to comply with this characteristic presents a penalty given by a formula proposed by the Federal Electricity Commission and is reflected in the receipt of this same company (CRE, 2019).

The problem that is presented nowadays arises from a previous situation in which the power factor was even lower, and the installation of a 160kVAr capacitor bank was implemented as the answer to the problem, however, as previously described, the results did not exempt the company from non-compliance with the requirement.

On the other hand, in the last years, there have been successful cases in various companies that provide service to the industry, which have achieve to increase the power factor by generating a bonus instead of a penalty.

Capacitor banks were installed in the company that produces and markets candy, managing to eliminate the penalty for the power factor (2020). The pet food development company was asked to connect a 620kVAr harmonic filter with the same objective (2019) and for the company dedicated to plastic extrusion and chrome plating, a capacitor bank was installed, achieving to increase the power factor to 0.98pf and mitigate the economic losses generated by the penalty (2019) (IEEE, 2012; Astudillo-Mora, 2016).

In all these reference cases, a constant was found which is the central point of this project, the previous analysis carried out on the quality of electrical energy. Carrying out the measurement of the electrical parameters allowed to know the relevant characteristics of the installed system, finding the problems to be solved and granting a personalized solution to each one of the cases presented.

Justification

When making a study of the quality of electrical energy, it is possible to know the state of the installation during its operation at the time of carrying out the measurements in a company. At the same time, the measurements provide information that, based on an analysis supported by regulations, stand out the following problems: a) Imbalances, b) low power factor, c) harmonics, d) current peaks, e) voltage drop.

The aforementioned situations result in considerable economic losses, such as additional charges in the payment of the receipt for penalties or fines depending on the applicable rate, loss of useful life or total loss of equipment installed in the plant, unscheduled shutdowns, stoppage of production lines, or even more alarming, accidents or human losses.

ISSN 2523-2881

On the other hand, by not having a good quality of electrical energy, consumption is higher, so generation must increase, and it pollutes mainly by thermal power plants that, through the burning of fossil fuels, produce CO_2, causing air pollution, by nuclear energy that causes radioactive waste from highly expensive treatments or by combined cycles that impact through combustion, in deposits, contamination of water, soil and ecosystems.

Topographic Analysis of the Network and Verification on the Point to be Evaluated

In order to carry out the corresponding operations to compare the results with the requirements described in the standards, it is necessary to obtain relevant data from the transformer which will be evaluated.

On the other hand, it is necessary to take into account the elements that are before and after the transformer, which is why the following single-line diagram is presented, showing the connection, the fuse, the transformer, the installed capacitor bank, the thermomagnetic switch and the electric board. The mentioned elements are in the same order from top to bottom in Figure 1.

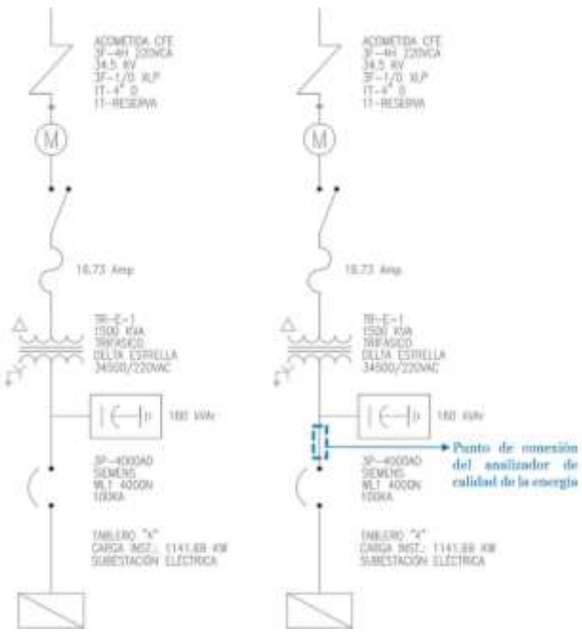

Figure 1 Single-line diagram of company's installation
Source: Own Elaboration

Measurement of Electrical Parameters in the Found System

By the time of carrying out the corresponding measurements, it was found that the system already had a capacitor bank that was intended to function as a solution to the low power factor, so the readings included this element. The following are the results:

Tension First Measurement

For voltage variations, the Regulatory Manual of Technical Requirements for the Connection of Load Centers is taken into account, where it is determined that these should not exceed ±5% with respect to the nominal voltage value. For this case the reference value is 220V (CRE, 2019). Table 1 shows the values obtained.

Ph	Tension (V)			Variation		Reg
	Min.	Rng.	Max.	Min.	Max.	
AB	217.57	224.65	226.44	1.1	2.9	Yes
BC	217.27	223.14	226.16	1.2	2.8	Yes
CA	217.78	224.48	226.63	1.0	3.0	Yes

Table 1 Verification of compliance of the regulation of tensión
Source: Own Elaboration

Current First Measurement

The occupancy percentage shows the breakdown by phases with respect to the total capacity. It is of high importance to have these values in order to not exceed them when increasing the installed load and moreover, to be able to verify that they are balanced (Ceballos, 2020), see Table 2.

Ph	Current (A)			Ocupation	
	Min.	Rng.	Max.	Min.	Max.
A	820	1,125	1,857	20.8	2.9
B	806	1,184	1,184	20.5	2.8
C	802	1,146	1,146	20.4	3.0

Table 2. Porcentage of current occupation respecto f the máximum capacity of the circuit (3,936A)
Source: Own Elaboration

The maximum occupancy percentage is 47.8% in Phase A, 50.2% in Phase B, 48.2% in Phase C, hence it is considered a good balance of Phases and there is a considerable percentage of occupancy left in case the user wants to increase the load (Ceballos, 2020).

ISSN 2523-2881

Frequency First Measurement

The frequency complies with the guidelines described in the Regulatory Manual of Technical Requirements for the Connection of Load Centers, since it mentions that the maximum permanent frequency must be 61Hz and a minimum of 59Hz, and in this case, its behavior is from 60.087Hz to 59.881Hz (CRE, 2019).

Energy Consumption First Measurement

The energy consumed (active power) is adequately higher than the lost energy (reactive power) and close to the apparent energy in the circuit (apparent power).

Table 3 shows the values obtained in the measurement, the active power that is the one used, the apparent power required for the operation of the system and the reactive power that is released in the use of energy. These values have a high relevance in the study because the relationship between them will reveal the value of the power factor, as well as other important parameters (Ceballos, 2020).

Power	Measured Values		
	Min.	Rng.	Max.
Apparent (KVA)	316	445.06	738
Active (kW)	290	412.87	700.2
Reactive (kVAr)	115.2	152.04	256.2

Table 3 Measured powers
Source: Own Elaboration

Power Factor First Measurement

We can observed that the average value is 0.83pf, however, for this parameter to be within the permissible limits, the value that is 95% of the time in the period must be taken into account, which is in this case 0.94pf (CRE, 2019).

Despite the fact that this value is considerably acceptable, it is not within the limits described in the Manual of Technical Requirements for the Connection of Load Centers that appears in the Network Code of the resolution of the Energy Regulatory Commission, since this mentions that it should be a value of 0.95pf (CRE, 2019).

Harmonic Dsitortion First Measurement

In relation to what is described in CFE L000-45 on the maximum limits of total harmonic distortion in voltage and individual harmonic component, there is no non-compliance with the regulation, see Table 4 and 5 (Blooming, 2006; IEEE, 1993; CFE, 2005).

Ph	THDV%	Limit	Reg
A	2.624	8%	Yes
B	2.416	8%	Yes
C	2.332	8%	Yes

Table 4 Verification of compliance of voltage total harmonic content per phase
Source: Own Elaboration

H order	Fundamental Value (%)			Limit	Reg
	A	B	C		
3°	0.168	0.119	0.148	6%	Yes
5°	0.995	0.961	0.936	6%	Yes
7°	1.472	1.383	1.486	6%	Yes
9°	0.151	0.165	0.189	6%	Yes
11°	1.589	1.313	1.097	6%	Yes

Table 5 Verification of compliance of voltage harmonic order per phase
Source: Own Elaboration

The CFE L000-45 standard is taken into account again to verify compliance with the values obtained, as described in the Table of maximum harmonic distortion allowed in current. Below are the results in which it is observed that there is a non-compliance of regulations, see Table 6 and 7 (Blooming, 2006; IEEE, 1993; CFE, 2005).

Ph	THDI%	Limit	Reg
A	10.183	5%	No
B	9.844	5%	No
C	8.446	5%	No

Table 6 Verification of compliance of current total harmonic content per phase
Source: Own Elaboration

H order	Fundamental value (%)			Limit	Reg
	A	B	C		
3°	0.506	0.666	0.683	4%	Yes
5°	2.159	2.143	2.195	4%	Yes
7°	3.608	3.279	3.331	4%	Yes
9°	0.558	0.442	0.735	4%	Yes
11°	8.101	7.620	6.069	2%	No

Table 7 Verification of compliance of current harmonic order per phase
Source: Own Elaboration

ISSN 2523-2881

Unbalance First Measurement

The CFE L000-45 standard mentions that the maximum voltage unbalance percentage allowed is 3%, which is why it is determined that the values comply with what is permissible (CFE, 2005).

In the CFE L000-45 standard it is mentioned that the maximum current unbalance percentage allowed is 5%, which is why it is determined that the values do not comply with what is permissible (CFE, 2005).

However, these values can be highly impacted when there is no load and in the points where it shows a higher imbalance there are no loads in operation, so the current imbalance percentage is not significant.

Summary of Results First Measurement

Tension. Phase imbalance does not exceed 3% allowed, so it is in safe operating conditions. The voltage regulation is within the standards.

Current. The maximum and minimum values are within the capacity of the circuit and current peaks that could trigger the electrical protections were not detected.

Power. The maximum power values are below 80% capacity of the transformer, which is why it is considered normal operation.

Power factor. It is below the established standards.

Harmonics. Within the readings carried out, the results show that the circuit is being affected by the presence of current harmonics.

With the summary of the results shown above, it is recommended to include a harmonic filter, however, since the system already has a capacitor bank, it is not possible to add it because it is not appropriate to place a correction element where one already exists, since that in each of the various brands that exist on the market, the behavior of the capacitor in micro farads varies, and even if it were of the same brand, if a filter or a capacitor is added, the inductance and capacitance would increase, making the calculation of these elements no longer correct due to the change in the characteristics of the circuit (Astudillo-Mora, 2016; IEEE, 2012).

This is why it is necessary to perform a second measurement by removing the bank of operation capacitors.

Second Measurement of Electrical Parameters with Capacitor Bank Out of Operation

Tension Second Measurement

For voltage variations, it is determined that they should not exceed ±5% with respect to the nominal value. For this case the reference value is 220V (CRE, 2019). The values obtained are shown below, see Table 8.

Ph	Tension (V)			Variation		Reg
	Min.	Rng.	Max.	Min.	Max.	
AB	215.07	222.33	231.16	2.2	5.1	Yes
BC	214.07	222.27	231.15	2.7	5.1	Yes
CA	215.25	222.51	231.24	2.1	5.1	Yes

Table 8 Verification of compliance of voltaje standard with a capacitor bank out of operation
Source: Own Elaboration

Current Second Measurement

The occupancy percentage shows a breakdown by Phases with respect to the total capacity, these current values can be seen in Table 9. It is of high importance to have these values in order to not exceed them when increasing the installed load and, moreover, to be able to verify that they are balanced (Ceballos, 2020).

Ph	Current (A)			Ocupation	
	Min.	Rng.	Max.	Min.	Max.
A	475	1,211	1,862	12.06	47.3
B	429	1,210	1,923	10.89	48.8
C	478	1,207	1,860	12.14	47.2

Table 9 Percentage of current occupation respect to the maximum capacity of the circuit (3,936A) with capacitor bank out of operation
Source: Own Elaboration

The maximum occupancy percentage is 47.3% in Phase A, 48.8% in Phase B, 47.2% in Phase C as shown, so it is considered a good balance of Phases and a considerable percentage of occupancy remains (Ceballos, 2020).

ISSN 2523-2881

Frequency Second Measurement

The frequency complies with the guidelines described, since it does not exceed the range of 61Hz to 59Hz, with 60.086Hz and 59.908Hz being the maximum and minimum respectively (CRE, 2019).

Energy Consumption Second Measurement

The energy consumed (active power) is adequately higher than the lost energy (reactive power) and close to the apparent energy in the circuit (apparent power), see Table 10.

Power	Measured Values		
	Min.	Rng.	Max.
Apparent (KVA)	184.2	463.04	705.3
Active (kW)	147.9	392.15	633.3
Reactive (kVAr)	103.8	152.04	360.9

Table 10 Measured powers with capacitor bank out of operation
Source: Own Elaboration

Power Factor Second Measurement

It is observed that the average value is 0.84, however, for this parameter to be within the permissible limits, the value that occurs 95% of the time in the period must be taken into account, which in this case is of 0.86 (CRE, 2019). This value is not within the limits described, since it is mentioned that it should be a value of 0.95 (CRE, 2019).

Harmonic Distortion Second Measurement

In relation to what is described in CFE L000-45 on the maximum limits of total harmonic distortion in voltage and individual harmonic component, the following results are presented, in which the percentage values of harmonic distortion are broken down, there is no non-compliance of the regulation (Blooming, 2006; IEEE, 1993; CFE, 2005), see Table 11 and Table 12.

Ph	THDV%	Limit	Reg
A	1.5	8%	Yes
B	1.532	8%	Yes
C	1.496	8%	Yes

Table 11 Verification of compliance of total voltage harmonics per phase with capacitor bank out of operation
Source: Own Elaboration

H order	Fundamental value (%)			Limit	Reg
	A	B	C		
3°	0.101	0.061	0.053	6%	Yes
5°	0.835	0.869	0.853	6%	Yes
7°	0.899	0.861	0.843	6%	Yes
9°	0.038	0.028	0.045	6%	Yes
11°	0.612	0.668	0.649	6%	Yes

Table 12. Verification of compliance by voltage harmonic order in each phase with capacitor bank out of operation
Source: Own Elaboration

The CFE L000-45 standard is taken into account again to verify compliance with the values obtained. The results are presented below in Tables 13 and 14, in which no non-compliance with regulations is observed (Blooming, 2006; IEEE, 1993; CFE, 2005).

Ph	THDI%	Limit	Reg
A	1.932	5%	Yes
B	1.958	5%	Yes
C	1.926	5%	Yes

Table 13 Verification of compliance of total current harmonics per phase with capacitor bank out of operation
Source: Own Elaboration

H order	Fundamental value (%)			Limit	Reg
	A	B	C		
3°	0.375	0.412	0.512	4%	Yes
5°	1.206	1.315	1.208	4%	Yes
7°	1.014	0.926	0.960	4%	Yes
9°	0.108	0.108	0.132	4%	Yes
11°	0.586	0.532	0.564	2%	Yes

Table 14. Verification of compliance by current harmonic order per phase with capacitor bank out of operation,
Source: Own Elaboration

Unbalance Second Measurement

In the CFE L000-45 standard it is mentioned that the maximum allowable percentage of unbalance in voltage is 3% and current is 5%, which is why it is determined that the measured values comply with what is permissible (CFE, 2005).

Summary of Results Second Measurement

Tension. Phase imbalance does not exceed 3% allowed, so it is in safe operating conditions. The voltage regulation is within the standards.

Current. The maximum and minimum values are within the capacity of the circuit and current peaks that could trigger the electrical protections were not detected.

ISSN 2523-2881

Power. The maximum power values are below 80% capacity of the transformer, which is why it is considered normal operation.

Power factor. It is below the established standards.

Harmonics. Within the readings carried out, the results show that the circuit was being affected by the presence of current harmonics while the capacitor bank was in place, now that this element has been removed, the harmonics also decreased in such a way that they are within the established limits.

Solution Proposal for Non-Compliance with the Electrical Quality Regulations at the Installation

With the summary of the results shown above, it is observed that, having the capacitor bank connected, the circuit needs to add inductance since, due to the lack of this, the current harmonic content increased considerably. An element that adds inductance and capacitance at the same time is a harmonic filter, which is why it is considered an effective response to the problem (Astudillo-Mora, 2016).

For this case, an automatic passive filter is taken into account that is capable of providing a low impedance path for current harmonics and is made up of an RLC branch in series. The filter will be connected in parallel with the power system (Astudillo-Mora, 2016).

Harmonic Filter Calculation

Data:
Active power = 633,300W
Current power factor = 0.73pf
Desire power factor = 0.98pf
Tension Phase-Phase = 220V
Fundamental frequency = 60Hz
Apparent power = 705,300VA

The minimum value of the measured power factor is 0.73pf, to carry out the design it is proposed to raise this value up to 0.98pf with reference to the Regulatory Manual of Technical Requirements for the Connection of Load Centers where it is specified that the power factor of 0.95pf will be valid for 10 years, after which the requirement will be 0.97pf (CRE, 2019). The power in the capacitor for an 11th order filter is calculated below.

$$\emptyset 1 = cos^{-1}(FP1) = cos^{-1}(.73) = 43.11° \quad (1)$$

$$\emptyset 2 = cos^{-1}(FP2) = cos^{-1}(.98) = 11.47° \quad (2)$$

$$Qeff = P(tan\emptyset 1 - tan\emptyset 2) \quad (3)$$

$$Qeff = 633.3kW(\tan(43.11) - \tan(11.47)) = 464{,}317.102VAr \quad (4)$$

Corresponding to the IEEE 18-2012 standard, the capacitor bank must be selected with respect to the established values (IEEE, 2012). Taking this into account and the possible increase in installed loads, a 500,000VAr capacitor bank is established. The arrangement is made up of a 166.6kVAr capacitor per branch, making a total of 500kVAr triphasic. The remaining calculations are shown in the following formulas.

$$xfilter = \frac{Vnom^2}{VAr} = \frac{220^2}{166{,}66kVAr} = 0.2904\Omega \quad (5)$$

The tuning factor used is 0.95 to avoid resonance due to the impedance of the network or the load used.

Capacitive reactance calculation:

$$xcap = \frac{h^2}{h-1} \cdot xfilter = \frac{10.45^2}{10.45-1} \cdot 0.2904 = 3.35581\Omega \quad (6)$$

Angular frequency calculation:

$$W = 2\pi fh = 2\pi(60)(10.45) = 3.35581 \quad (7)$$

Capacitor calculation:

$$C_{farads} = \frac{1}{W \cdot xcap} = \frac{1}{3{,}939.5 \cdot 3.355} = 76.0941525\mu F \quad (8)$$

Inductive reactance calculation:

$$xL = \frac{xcap}{h^2} = \frac{0.0307301573}{10.45^2} = 0.03073\Omega \quad (9)$$

Inductor calculation:

$$L_{henries} = \frac{xL}{W} = \frac{0.03073}{3{,}939.5} = 0.0078mH \quad (10)$$

Resistence calculation:

$$R = \frac{x_L}{U} \equiv \frac{0.03073}{80} = 0.384126966m\Omega \quad (11)$$

The characteristics for the harmonic filter are summarized in Table 15.

Conection	Star
Power per branch (VAr)	166,666.667
Tension (V)	220
Inductor L (mH)	0.00780040898
Capacitor C (F)	76.0941525
Resistence R (mΩ)	0.384126966

Table 15 Characteristics for the harmonic filter
Source: Own Elaboration

Harmonic Filter Simulation

To verify the veracity of these data, a model was made in DigSILENT Power Factory with the characteristics of the initial network where, when simulating the harmonic content, it provided values very similar to those obtained in the measurements (Astudillo-Mora, 2016), see Figure 2.

A 1500 kVA transformer was added to the elements, and together with the harmonics and the load, the simulation gave values of 633kW in active power, 360kVAr in reactive power, 728kVA in apparent power and 0.86pf in power factor. These values are highly similar to those obtained in the measurements actually carried out on the system.

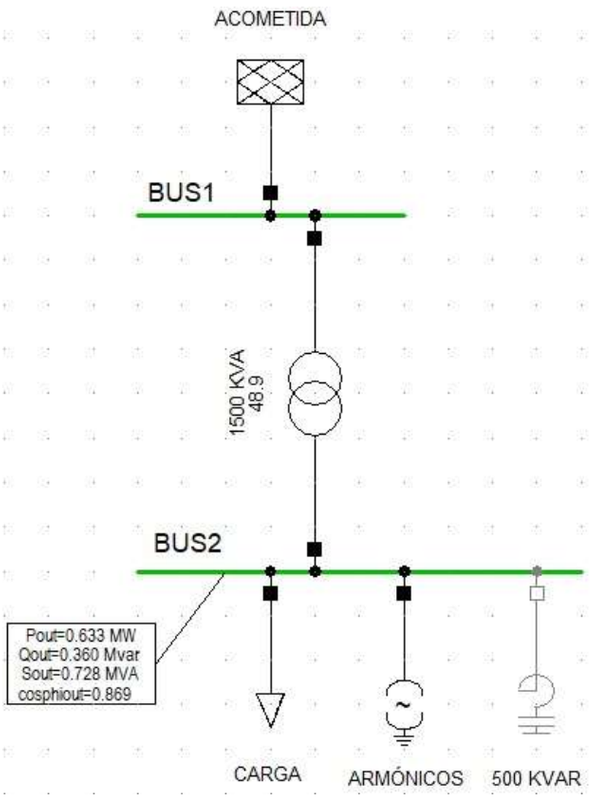

Figure 2 Diagram of the simulated system in DigSILENT Power Factory before applying the solution proposal
Source: Own Elaboration

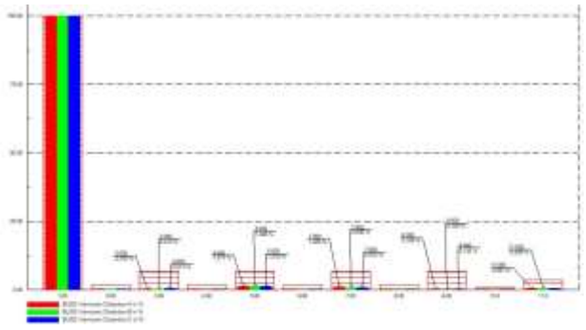

Figure 3 Simulated harmonic content in DigSILENT Power Factory before applying the proposed solution
Source: Own Elaboration

The closeness of the simulated harmonics that are observed in Figure 3, with respect to the values measured in the facilities, confirms that the software has the capacity to emulate the characteristics that the electrical system would generate in case of making any modification.

H order	Simulated harmonic content			Measured harmonic content		
	A	B	C	A	B	C
3°	0.38	0.41	0.51	0.38	0.41	0.51
5°	1.22	1.37	1.22	1.21	1.32	1.21
7°	1.03	0.94	0.97	1.01	0.93	0.96
9°	0.11	0.11	0.13	0.11	0.11	0.13
11°	0.59	0.54	0.56	0.59	0.53	0.56

Table 16 Comparison of the simulated and measured values
Source: Own Elaboration

The values taken for the measured harmonic content show a minimal variation in decimals of the simulated harmonic content values, this comparison is shown in Table 16. These were taken from the measurement made with the capacitor bank disconnected, therefore these are values that do not exceed the permissibe limit, however, it is necessary to analyze that, in the measurement made with the capacitor bank connected, the current harmonic of order 11 was highly affected.

Figure 4 shows the results that would be obtained in case of placing the harmonic filter sized at 500kVAr.

ISSN 2523-2881

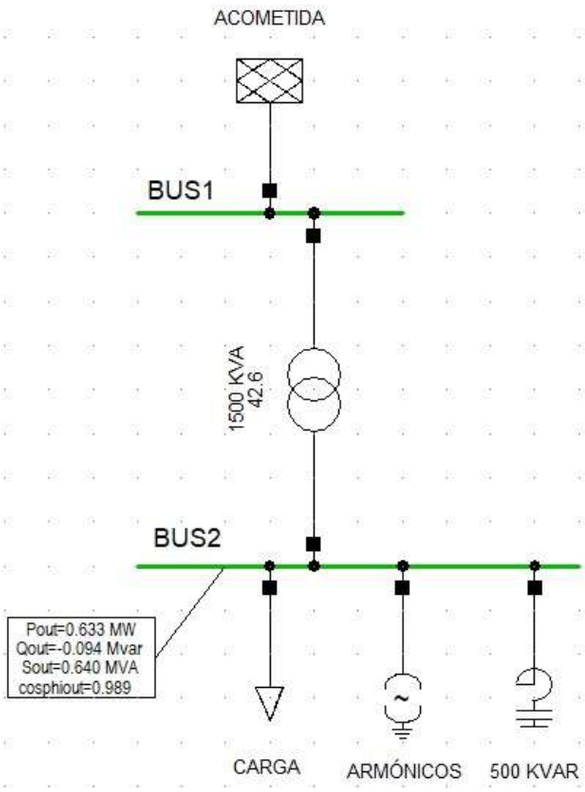

Figure 4 System diagram simulated in DigSILENT Power Factory with the harmonic filter activated
Source: Own Elaboration

It is observed that the active power in the system would be 633kW, the reactive power decreases from 360kVAr to 94kVAr, therefore the apparent power, in the same way, is affected by a decrease from 738kVA to 640kVA, and this effect causes the power factor that measures the effective use of electrical energy in the system increases to 0.98pf as expected.

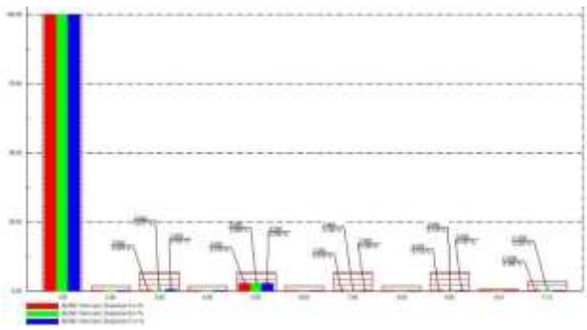

Figure 5 Simulated harmonic content in DigSILENT Power Factory with the harmonic filter activated
Source: Own Elaboration

The harmonics that are presented in Figure 5 are shown in Table 17. It is observed that these do not exceed the permissible limits in the regulations (Blooming, 2006; IEEE, 1993; CFE, 2005).

H order	Fundamental value (%)			Limit	Reg
	A	B	C		
3°	0.375	0.417	0.532	4%	Yes
5°	2.779	2.958	2.782	4%	Yes
7°	0.215	0.162	0.184	4%	Yes
9°	0.114	0.114	0.127	4%	Yes
11°	0.388	0.323	0.362	2%	Yes

Table 17. Verification of compliance with the standard by harmonic order with the harmonic filter activated
Source: Own Elaboration

Metodology

Considering the problem, it was evaluated that the best option to improve the quality of electrical energy is to first analyze the topography of the electrical system to determine the points where the parameter measurements will be made. In this way, it is possible to identify and specifically name those that are causing disturbances in the system, or are failing to comply with the applicable regulations in the case study.

To carry out the measurement, it is necessary to take readings for 7 continuous days as described in the CFE-L00045 standard with an electrical power quality analyzer regularly connected to the transformer or to the main distribution board, in this way it is possible to evaluate the general behavior of the electrical system of the company (CFE, 2005).

In this case, the system to be evaluated currently has a capacitor bank installed and in operation, however, the expected results were not obtained according to the regulations and technical requirements of electrical power quality, so the system is evaluated again disconnecting this element to know the behavior during its operation and thus be able to evaluate the parameters properly.

Once the measurements have been made and analyzed, we proceed to assess the resolution options for the diagnosed regulatory breaches by developing their respective simulation in the specialized software to verify the functionality of the proposal.

Results

The general objective has been covered in its entirety, because the breakdown of each of the electrical parameters shows that they have been analyzed and it is possible to determine a first state of the system.

ISSN 2523-2881

Having determined this state where there is a low power factor (CRE, 2019), shown in the summary of results with the capacitor bank disconnected, it is possible to issue a proposal that generates an improvement in energy quality, raising this value from 0.73pf to 0.98pf without increasing harmonic content. It is possible to observe this improvement in the model.

Conclusions

For this specific case study, it was necessary to place a new element, which is a 500kVAr automatic passive harmonic filter, which promotes an increase in the power factor and controls the percentages of harmonic content, keeping them below the levels allowed in the standards.

We can see the importance of first carrying out a power quality analysis since, without this, it would not have been possible to locate the problem that existed in the current harmonic content, and in general, in this analysis. It is possible to break down each of the parameters and visualize them in detail, finding the problem if there is one.

It is necessary to take into account that all the elements of an electrical installation must have a maintenance service annually to ensure that they continue to function satisfactory, which includes electrical evaluations, cleaning and readjustment of exhaustible resources or that deteriorate over time. In the same way, there must be a control where the loads to which the system is exposed are specified in order to be absolutely careful not to exceed the installed capacities.

Within the same recommendations, it is necessary to constantly update the single lines and load tables where it will be possible to observe the history of the changes that have been made in the electrical network, and in case of wanting to make a modification of any magnitude, have accessibility to those preceding states. On the other hand, this project reveals the importance of carrying out an energy quality analysis and, in turn, makes it impossible to make a proposal for a modification in the electrical network with the intention of improving quality without knowing a first state, since the effects can be counterproductive and cause the quality of electrical power to deteriorate.

In case of wanting to carry out an analysis of the quality of electrical energy, it is recommended to use the same procedure in question of prioritizing the analysis, however, the proposals for improvement will be conditioned to each of the cases found in the field, since which all vary in installed loads and individual system characteristics.

Carrying out this study covers a wide range of topics of importance in the behavior of energy. The power factor is not only a requirement that, if it is not met, generates an economic penalty, but it is a value which provides information about how much electrical energy is truly used, and how much is being lost, so that by its nature it causes pollution in the environment.

This analysis is responsible for pinpointing where energy is being wasted, where there are points where an immediate fix is required, and which of them present an area of opportunity in order to the energy does not continue to be wasted, and that which is generated is consumed efficiently.

References

Astudillo-Mora, L., Vásquez-Vega, A., Rojas-Serrano, J. (2016). Implementación de un filtro pasivo para compensación armónica y corrección del factor de potencia. Científica, vol. 20, núm. 1. ESIME Instituto Politécnico Nacional México. https://www.redalyc.org/journal/614/61447568001/html/

Blooming, T. & Canovale, D. (2006) Application of IEEE STD 519-1992 Harmonic Limits, Conference Record of 2006 Annual Pulp and Paper Industry Technical Conference**,** Appleton, WI, USA, 2006, pp. 1-9, doi: 10.1109/PAPCON.2006.1673767.

Ceballos, F. (2020). Reporte de monitoreo de parámetros eléctricos. Tecsa Energy Expertise Querétaro.

Comisión Reguladora de Energía. (2019). Guía sobre los requerimientos técnicos del Código de Red aplicables a Centros de Carga. Comisión Reguladora de Energía.

ISSN 2523-2881

Comisión Federal de Electricidad. (2005). Desviaciones permisibles en las formas de onda de tensión y corriente en el suministro y consumo de energía eléctrica. Comisión Federal de Electricidad. https://lapem.cfe.gob.mx/normas/pdfs/v/L0000-45.pdf

"IEEE Standard for Shunt Power Capacitors," in TA Std 18-2012 (Revision of IEEE Std 18-2002), vol., no., pp.1-39, 15 Feb. 2013, doi: 10.1109/IEEESTD.2013.6466331

"IEEE Recommended Practice and Requirements for Harmonic Control in Electric Power Systems," in IEEE Std 519-2014 (Revision of IEEE Std 519-1992), vol., no., pp.1-29, 11 June 2014, doi: 10.1109/IEEESTD.2014.6826459.

ISSN 2523-2881

Article **Journal Renewable Energy**
December, 2023 Vol.7 No.19 12-18

Design and construction of a solar simulator for characterization of photovoltaic modules

Diseño y construcción de un simulador solar para caracterización de módulos fotovoltaicos

LÓPEZ-CARRILLO, José Luis, GARCÍA-PEDROZA, Luis Daniel, REYES-DURÁN, Bernardo and ÁLVAREZ-MACÍAS, Carlos*

Tecnológico Nacional de México/Instituto Tecnológico de la Laguna, Torreón 27000, Coahuila, México

ID 1er Author: *José Luis, López-Carrillo* / **ORC ID**: 0000-0003-0860-2164, **CVU CONAHCYT ID**: 1243944

ID 1er Co-author: *Luis Daniel, García-Pedroza* / **ORC ID**: 0000-0003-0816-4918, **CVU CONAHCYT ID**: 1243933

ID 2do Co-author: *Bernardo, Reyes-Durán* / **ORC ID**: 0000-0001-6006-0361, **CVU CONAHCYT ID**: 94905

ID 3er Co-author: *Carlos, Álvarez-Macías* / **ORC ID**: 0000-0002-2263-0316

DOI: 10.35429/JRE.2023.19.7.12.18 Received July 30, 2023; Accepted October 30, 2023

Abstract

This work comprises the design, development, characterization and implementation of a solar simulator prototype for photovoltaic modules, implementing LED lamp technology as artificial lighting. First, we designed the prototype in AutoCAD, and then we built it using a box (100×100×35cm) made of sheet metal as a cabin. We used a super polished sheet as a reflective surface inside the cabin. Inside the cabin, we placed 8 LED lamps of 200 and 50 Watts in order to have a constant irradiance. An Arduino UNO board and a SPLITE2 pyranometer were used to measure lamp irradiance, along with a MATLAB data acquisition system. As a result, a functional prototype of a CB type solar simulator with an area of 1m^2 was got with a constant irradiance of 200 W/m^2 at a height of 30cm and with a homogeneity of 98.6 W/m^2 difference between peaks.

Solar simulator, Irradiance, LED technology, Characterization, Prototype

Resumen

Este trabajo consiste en el diseño, desarrollo, caracterización e implementación de un prototipo de simulador solar para módulos fotovoltaicos, implementando tecnología de lámparas LED como iluminación artificial. Primero se realizó el diseño del prototipo en AutoCAD, posteriormente, se construyó utilizando una caja (100×100×35cm) de lámina como cabina, la cual en el interior cuenta con lamina superpulida utilizada como superficie reflejante. En el interior de la cabina se colocaron 8 lámparas LED de 200 y 50 Watts con la finalidad de tener una irradiancia constante. Se utilizó un piranómetro SPLITE2 adaptado con una tarjeta Arduino UNO para caracterizar la irradiancia de las lámparas dentro de la cabina, así como un sistema de adquisición de datos en MATLAB. Como resultado se obtuvo un prototipo funcional de un simulador solar tipo CB de área de 1m^2 con una irradiancia constante de 200 W/m^2 a una altura de 30cm y con una homogeneidad de 98.6 W/m^2 de diferencia entre picos.

Simulador solar, Irradiancia, Tecnología LED, Caracterización, Prototipo

Citation: LÓPEZ-CARRILLO, José Luis, GARCÍA-PEDROZA, Luis Daniel, REYES-DURÁN, Bernardo and ÁLVAREZ-MACÍAS, Carlos. Design and construction of a solar simulator for characterization of photovoltaic modules. Journal Renewable Energy. 2023. 7-19: 12-18

*Correspondence to Author (e-mail: calarezm@correo.itlalaguna.edu.mx)
† Researcher contributing as first author.

Introduction

To properly understand the operation of the solar cell, it is necessary to take into consideration the influence of the two main external factors: the ambient temperature (Perpiñán, 2015) and incident illumination

Solar simulators are indispensable tools in the characterization of photovoltaic modules. These simulators present controlled conditions of radiation and temperature. For these reasons laboratory tests, under controlled conditions, can provide more reliable information, the radiation variation of a solar simulator can be performed by different techniques depending on the technical characteristics of the lamps used. (Bodnár, 2020)

In order to perform experimental tests with photovoltaic modules, an operation must be maintained under established standards, in standard measurement conditions SCT (Standard Test Conditions), which correspond to an irradiance in the module plane of 1,000 W/m2, module temperature of 25 ºC and a spectral distribution of irradiance according to the air mass factor AM 1.5 (Canales, 2004).

The aim was to develop a prototype solar simulator for the characterization of photovoltaic modules based on LED lamps, seeking to approach commercial versions. These devices present a good correlation compared to a solar simulator with a xenon lamp. Such a device presents a low cost and, in particular, an easy way to control the luminous flux.(Grandi, 2014).

Something to keep in mind, is the LED light emission spectrum. For a white LED, the normalized emission spectrum measured at room temperature consists of a blue peak located at approximately 450 nm emitted by the LED chips and a broad yellow peak at ~560 nm emitted by the phosphor particles. (Jeong, 2012) As shown in Figure 1.

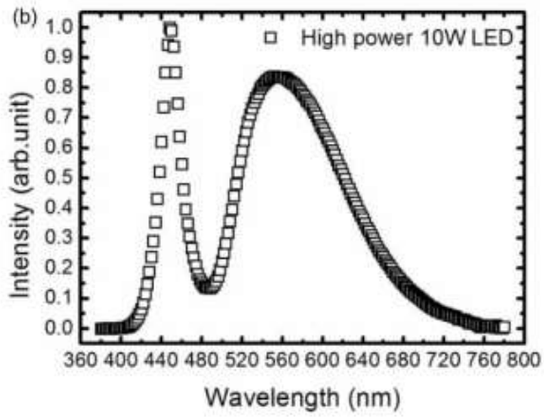

Figure 1 Emission spectrum White LED (Jeong, 2012)

The requirements for solar simulators are found in the American Standard for Testing and Materials (ASTM) E972. According to this standard, solar simulators can be classified by three main aspects and into different classes, A, B or C (Table 1) based on the three aspects mentioned above (Jeong, 2012). However, any solar simulator should be able to provide the average surface light intensity (AM 1.5) with a maximum value of 1000 W/m^2 (Jeong, 2012).

	Class A	Class B	Class C
Spectral conformity	75-125%	60-140%	40-120%
Spatial uniformity	≤2%	≤5%	≤10%
Temporary stability	≤2%	≤5%	≤10%

Table 1 Classification of solar simulators (Bodnár, 2020)

The spectrum is also characterized by the percentage of irradiance in eight wavelength intervals. Table 2 shows the standard terrestrial spectra of AM 1.5G (Global) and AM 1.5D (Direct) and the extraterrestrial spectrum AM 0. (Wang, 2014)

Length	**Total irradiance percentage**		
[nm]	AM1.5 D	AM1.5G	AM0
300-400	Not specified	Not specified	8.0%
400-500	16.9%	18.4%	16.4%
500-600	19.7%	19.9%	16.3%
600-700	18.5%	18.4%	13.9%
700-800	15.2%	14.9%	11.2%
800-900	12.9%	12.5%	9%
900-1100	16.8%	15.9%	13.01%
1100-1400	Not specified	Not specified	12.2%

Table 2 Percentage irradiance by wavelength. (Grandi, 2014)

ISSN 2523-2881

In this work, the design, construction, characterization and implementation of a first version of a solar simulator prototype for the characterization of photovoltaic modules, implementing LED lamp technology as artificial lighting, was carried out.

Methodology to be developed

For the construction of the system, a square wooden box of 1m per side and 35 cm high was used. Two different types of LED lamps were used at the bottom, two GOGOLITE GL-FG013 and six ZL-RS-50W. The height above the lamps was calculated to obtain a more uniform irradiance at a multiple of 1000 W/m2. To measure the irradiance inside the box, a Kipp and Zonen SP-Lite 2 pyranometer and a multimeter were used to interpret the values obtained by the pyranometer. Inside the box, aluminum foil was placed on each of the faces, in order to have a reflective effect which helps to have a better concentration of light (Figure 2a).

Three openings were made through which the pyranometer could be introduced and placed inside the analysis quadrants to perform the measurements inside the system. These openings are 30 cm high every 5 centimeters, in order to measure irradiance at 6 different heights and thus determine homogeneity (figure 2b).

Figure 2 A) inside of the test box. B) opening for the introduction of the pyranometer

Connections were made for the lamps powered by two 110V sources, one for the 6 ZL-RS-50W lamps (large) and the other for the GOGOLITE GL-FG013 lamps (small). Each of the arrays was connected in parallel, resulting in the arrangement shown in Figure 3.

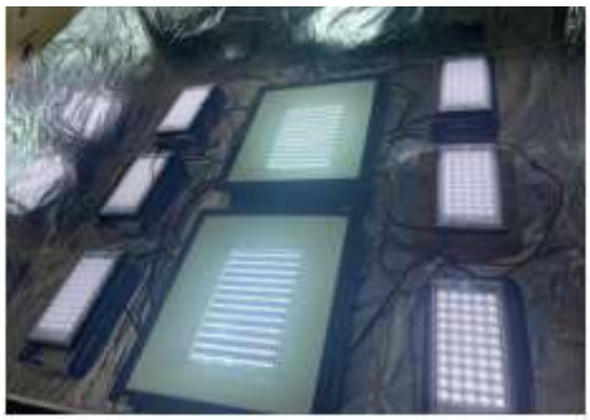

Figure 3 Lamp connection arrangement

With the location and distribution of the lamps and the dimensions of the box, we worked on the virtual design using the AutoCAD program shown in figure 4.

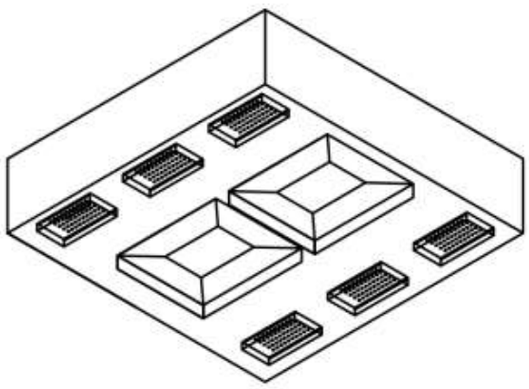

Figure 3 Arrangement of lamp connections

As spectroscopy tests, the pyranometer and a set of cellophane paper of different colors (red, yellow, green, blue and purple) were used to obtain the irradiance passing through each color, in order to speculate its irradiation spectrum (Figure 5).

Figure 5 Blue and purple spectroscopy tests

Subsequently, the construction of the simulator was carried out using the 1 meter per side and 35 centimeters high sheet metal box. Inside the box super polished foil was placed on the 4 walls (Figure 6a) which will do the same job as the aluminum in the test box, i.e., as a reflective surface to help have a more homogeneous radiation inside the system.

ISSN 2523-2881

Figure 6 A) cutting of super polished sheet for solar simulator walls. B) fixing of lamps inside the box

As can be seen in Figure 6b, angles and screws were used to fix the lamps, which go directly to the structure of the sheet metal box.

The irradiance measurements were repeated in the 9 quadrants in which the simulator surface was divided and where a more homogeneous irradiance was obtained at a height of 30 cm. Once the lamps were installed, the pyranometer and an Arduino were used to perform the measurements and analyze the data obtained more precisely (Figure 7a and 7b).

Figure 7 A) Final irradiance measurement. B) Pyranometer data collection

For the implementation stage, a photovoltaic module model EPCOM PRO1012 was used, obtaining its I-V characteristic curves by means of a PROVA 200A curve tracer (Figure 8), with which the 5 electrical parameters were obtained.

Figure 8 Characterization of photovoltaic module

Results

Graphs 1a, 1b, 1c and 1d show the distribution of irradiance emitted by the set of lamps within an area delimited by the 9 quadrants. The measurements were performed in a 3×3 coordinate system.

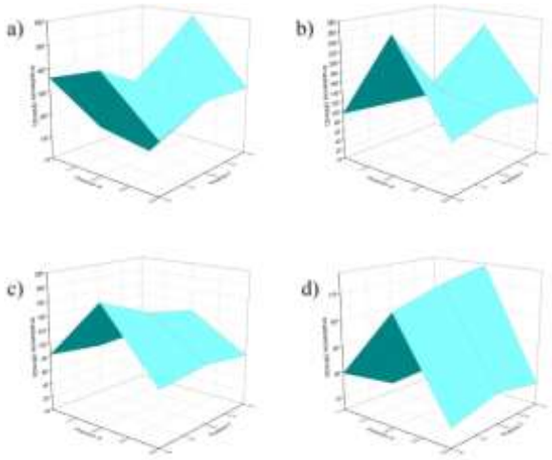

Figure 9 A) Irradiance distribution at 10 cm. B) Irradiance distribution at 20 cm. C) Irradiance distribution at 30 cm. D) Irradiance distribution at 35 cm

Graph 1 shows the irradiance intensities measured on the test prototype in the form of surfaces. It is observed that for surfaces A, B and D, there is non-uniformity in the irradiance and that in the case of surface C the irradiance becomes more uniform, at an average value of about 100 W/m2 (Annex A).

Analysis of measurements of the electromagnetic spectrum of LED lamps

The graph in Figure 10 shows the irradiance emitted by the white light of the two LED lamps, passing it through the colored cellophanes and recording its intensity with the pyranometer.

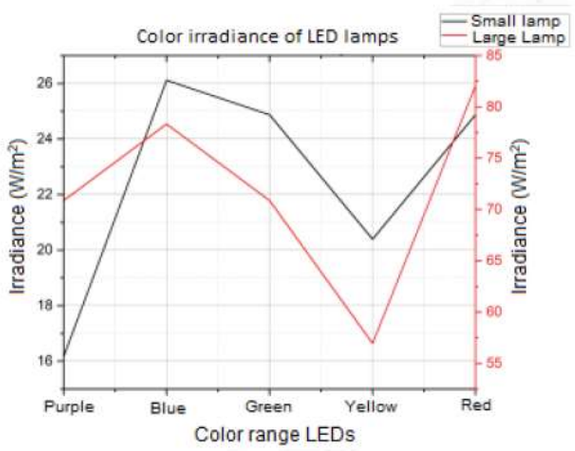

Figure 10 Characterization of the photovoltaic module

From figure 10 it is possible to observe the similar behavior for both lamps, which means that the LEDs are the same and only differ in the quantity that each lamp has, this because the difference between both curves is the intensity.

ISSN 2523-2881

On the other hand, for both cases, the predominant presence of blue, green and red colors, emitted by the white LED lamps, stands out. This behavior is consistent with Figure 1 where the theoretical emission spectrum of a white LED is observed.

Regarding the homogeneity of the irradiance in the system, the graph in Figure 11 shows the distribution of irradiance emitted by the array of LED lamps inside the solar simulator prototype, measured at a height of 30 cm above the lamps.

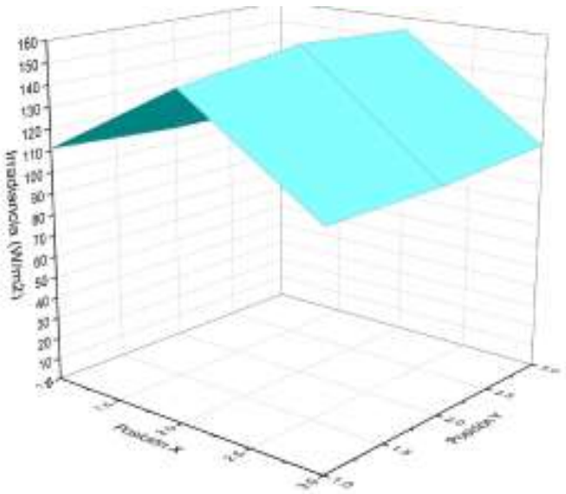

Figure 11 Irradiance distribution of the built solar prototype

As can be seen, the distribution in the prototype of the constructed solar simulator is more uniform than the irradiance distribution of the test prototype. In addition, an increase in the irradiance emitted by the LED lamps is observed due to the use of the super polished sheet on the walls of the system, despite maintaining the same arrangement of lamps.

Table 3 shows the irradiance measurements in each of the 9 quadrants of the solar simulator.

Quadrant	Irradiance (W/m^2)
1	111.1
2	149.2
3	105.2
4	106.9
5	157.3
6	105.2
7	106.3
8	154.2
9	108.6
Average	122.66

Table 3 Irradiance measured per quadrant of the prototype

Temperature analysis of the solar simulator prototype

The graph in Figure 12 shows the time variation curve of the temperature inside the solar simulator prototype. As can be seen, the adjustment shows an increase in the internal temperature of 1.46°C/minute, with this value it is possible to get an idea of how long the system has to be allowed to cool down to perform the next module characterization.

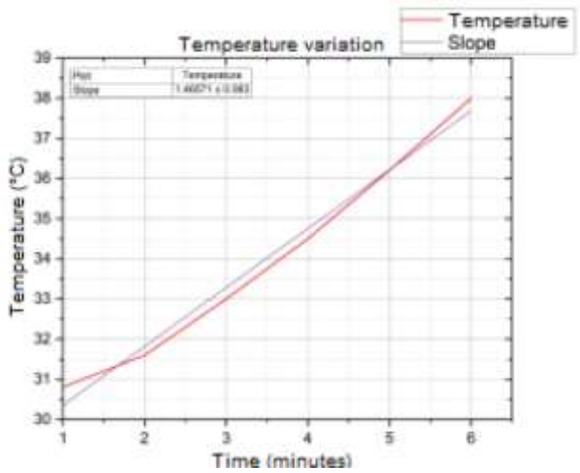

Figure 12 Temperature variation of the prototype

Characterization of the solar simulator prototype

Table 4 shows the wavelength irradiance percentages of the prototype compared to the irradiance of the sun at AM0 conditions. It is observed that the spectral conformity of the prototype is 53.57% which is a value corresponding to class C, the inequality of the prototype is 7.43% which corresponds to class B, so the final classification of the solar simulator prototype is class CB according to Table 1.

Wavelength [nm]	Percentage of total irradiance	
	AM0	Prototype
300 - 400	8%	11.48%
400 - 500	16.40%	9.57%
500 - 600	16.30%	23.37%
600 - 700	13.90%	
700 - 800	11.20%	9.35%
800 - 900	9%	
900 - 1100	13.10%	
1100 -1400	12.20%	
Spectral conformity with respect to sunlight	100%	53.77%
Class	A	C
Spatial inequality	0%	7.43%
Class	A	B

Table 4 Comparison with AM0 values of the irradiance per wavelength

ISSN 2523-2881

Implementation of the system on a photovoltaic module

The graph in Figure 13 shows the I-V characteristic curve of a photovoltaic module model EPCOM PRO-1012 irradiated with the prototype built with the solar simulator, the values obtained are compared with the curve at STC conditions of its data sheet (see Annex B).

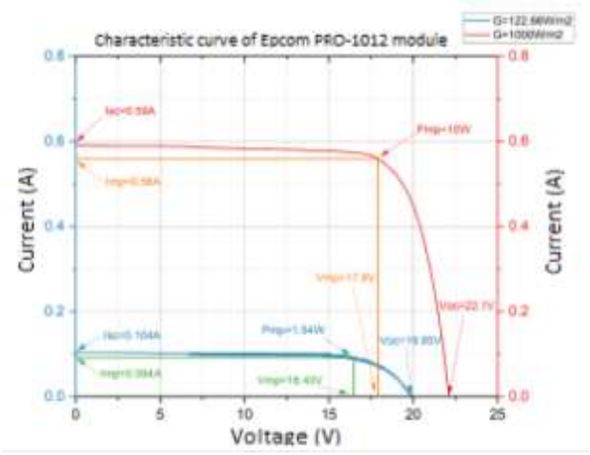

Figure 13 Characteristic curves of the photovoltaic module

As can be seen, the characteristic curve obtained with the use of the solar simulator has the same behavior as the characteristic curve provided by the technical data sheet of the photovoltaic panel. With this it can be concluded that the simulator has a uniform irradiance and works to obtain the values of the parameters used for the definition of the characteristic curve at a lower irradiance.

Annexes

Annex A. Measurements taken on the test prototype.

Cuadrante/Altura	10 cm	15 cm	20 cm	25 cm	30 cm	35 cm
1	360.60	139.26	94.50	85.79	83.31	79.58
2	441.43	364.33	272.32	216.36	172.84	106.93
3	222.58	82.06	103.20	80.82	78.33	72.12
4	62.17	145.48	118.12	87.04	74.60	68.39
5	18.65	92.01	135.53	140.51	141.75	113.15
6	308.38	185.27	123.10	94.50	85.79	77.09
7	264.85	92.01	105.60	80.82	78.33	69.63
8	584.43	322.05	252.42	182.79	128.07	116.88
9	299.67	187.76	110.66	83.31	75.85	73.36
Promedio	284.75	178.92	146.17	116.88	102.10	86.32

Nota: Valores registrados en W/m^2

Annex B. EPCOM PRO-1012 photovoltaic module datasheet

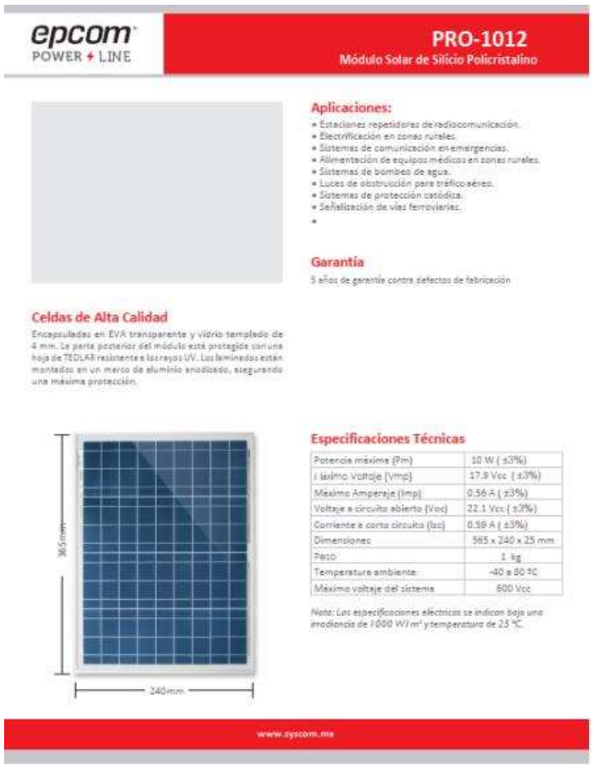

Acknowledgment

Thanks to the Tecnológico Nacional de México for the use of the facilities of the La Laguna campus. The authors are grateful for the support financed by TecNM and PRODEP projects. Special thanks to CONAHCYT for grants; CVU 1243944 José Luis López Carrillo, CVU 1243933, Luis Daniel García Pedroza and CVU: 94905, Bernardo Reyes Durán.

Conclusions

In this work, a solar simulator prototype was designed and built, which was characterized and used to obtain an electrical properties curve in a photovoltaic module. The analysis determines that the prototype built can be comparable to a solar simulator type CB, because it is close in the spectral conformity in simulator type C and in the spatial inequality in the AM0 spectrum of type B.

The height of 30 cm above the lamps was the optimum in the system to achieve the best radiation uniformity of magnitude 98.6 W/m2 within the area covered by the light from the lamps. Inside it was observed that the temperature rises 1.4 degrees per minute when the prototype is in operation, which presents a weakness of the simulator, a temperature control system is recommended to counteract the rise in temperature.

It was determined that the LED lamps of the prototype differ 46.23% with respect to the sun in terms of spectral conformity, and 7.43% in terms of spatial inequality, these results indicate that the prototype solar simulator class CB is suitable for experimental use, since it can approximate the sun in spectral and spatial terms.

References

[I] O. Perpiñán Lamigueiro, (2015). Energía Solar Fotovoltaica. México. https://github.com/oscarperpinan/esf

[II] Bodnár, I., Koós, P. y Skribanek, Á. (2020). Design and construction of a sun simulator for laboratory testing of solar cells. Acta Polytechnica Hungarica, 13:165–184. https://doi.org/10.12700/aph.17.3.2020.3.9

[III] Canales Be, G.M. (2004). Caracterización de un simulador solar. PhD thesis, División de Ciencias e Ingeniería, Universidad de Quintana Roo. http://hdl.handle.net/20.500.12249/651 http://risisbi.uqroo.mx/handle/20.500.12249/651

[IV] Grandi, G., Ienina, A., and Bardhi, M. (2014). Effective low-cost hybrid led-halogen solar simulator. IEEE Transactions on Industry Applications, 50:3055–3064. https://api.semanticscholar.org/CorpusID:18717939

[V] Jeong, S. y Ko, JH. (2012). Analysis of the spectral characteristics of white light-emitting diodes under various thermal environments. Journal of Information Display, 13. DOI.10.1080/15980316.2012.652254

[VI] Wang, W. y Laumert, B. (2014). Simulate a 'sun' for solar research: A literature review of solar simulator technology. https://api.semanticscholar.org/CorpusID:106667773

ISSN 2523-2881

Article **Journal Renewable Energy**
December, 2023 Vol.7 No.19 19-27

Design considerations for the dimensioning of parabolic trough solar thermal plants

Consideraciones de diseño para el dimensionamiento de plantas solares térmicas de concentrador parabólico

LIZÁRRAGA-MORAZÁN, Juan Ramón† & PICÓN-NUÑEZ, Martin

Department of Chemical Engineering, Division of Natural and Exact Sciences, University of Guanajuato, Mexico.

ID 1er Author: *Juan Ramón, Lizárraga-Morazán* / **ORC ID**: 0000-0002-7733-5621, **CVU CONAHCYT ID**: 83138

ID 1st Co-author: *Martin, Picón-Nuñez* / **ORC ID**: 0000-0002-0793-192X, **CVU CONAHCYT ID** 12408

DOI: 10.35429/JRE.2023.19.7.19.27 Received July 30, 2023; Accepted October 30, 2023

Abstract

Solar heaters of the parabolic trough type, PTC, are a proved technology that has a wide diversity of industrial applications. The prediction of the thermal conditions in these devices plays a fundamental role in the development and design of thermal plants capable of meeting the heat load requirements. To this end highly complex thermal models have been derived which are difficult to solve and implement. This work puts forward a PTC transient thermal model which was validated using experimental data and compared against other theoretical models existing in the open literature. Along with this model, a novel sequential solution procedure is proposed with which a better follow up of variable outputs is obtained. A parametric analysis was carried out of for the main design variables using the Present Value of the Life Cycle Energy Savings (PVLCES) and Total Integrated Heat (TIH) using daily typical data in the winter and summer seasons for the city of Guanajuato. Due to its transient nature, the model can be implemented in research where optimisation tools are required such as Deep Learning, Machine Learning and Control, which are basic in the dimensioning of thermal solar plants.

Parabolic trough solar collectors, Thermal design, Thermal performance, Solar field sizing, Solar thermal energy

Resumen

Los calentadores solares tipo parabólico, PTC, son una tecnología ya probada con una gran diversidad de aplicaciones industriales. La predicción de las condiciones térmicas de estos equipos juega un papel fundamental para el desarrollo y diseño de plantas termosolares capaces de cumplir con los requerimientos y cargas térmicas. Con este fin se han desarrollado modelos térmicos altamente complejos que presentan dificultades para su implementación y solución. En este trabajo se propone un modelo térmico para la tecnología PTC en estado transiente unidimensional, que fue validado con datos experimentales y comparado con otros modelos existentes en literatura. Con el modelo, se propone un procedimiento novedoso de solución de tipo secuencial, con el que se tiene un mejor seguimiento de los resultados de las variables. Se realizó un análisis paramétrico de las principales variables de diseño del equipo empleando como indicadores el Valor Presente del Análisis del Ciclo de Vida (PVLCES por sus siglas en inglés) y el Calor Total Integrado (TIH por sus siglas en inglés) con datos diarios típicos estacionales de invierno y verano para la ciudad de Guanajuato. Dada su naturaleza transiente, el modelo puede ser implementado para el desarrollo de investigaciones que requieran el empleo de las herramientas de optimización, Deep Learning, Machine Learning y de Control, que actualmente son básicas en el dimensionamiento de estas redes termosolares.

Colectores solares de tipo parabólico, Diseño térmico, Desempeño térmico, Dimensionamiento de campos solares, Energía solar térmica

Citation: LIZÁRRAGA MORAZÁN, Juan Ramón & PICÓN-NUÑEZ, Martin. Design considerations for the dimensioning of parabolic trough solar thermal plants. Journal Renewable Energy. 2023. 7-19: 19-27

* Author Correspondence (e-mail: lizarragamorazan@hotmail.com)
† Researcher contributing as first author.

Introduction

The constant growth of industrial activity is a core issue for counties to achieve its economical sustainability. Such development goes hand in hand with energy consumption. According to IEA (International Energy Agency), the share of the industrial sector is 32 % of the total energy consumption [I]. International agreements and the 2030 UN agenda foster the use of clean energy to curb environmental pollution. The economic reactivation after the Covid-19 pandemic and the response to the global energy crisis have driven investment in clean energy, reaching 1.7 trillion USD over the first half of 2023; with fossil energy investment of only about 0.9 trillion USD [II]. It is foreseen that the substitution of fossil fuel by clean energy will be achieved by 2050, although it depends on the implementation and the support of suitable local and international policies [III].

Solar energy is a limitless and clear energy source that is harnessed employing technologies referred to as SHIP (solar heat for industrial processes) that include CSP (concentrated solar power), PV (photovoltaic), solar Chemistry, solar desalination, and solar cooling amidst others [IV], [V]. The total installed accumulated capacity in operation by the end of 2022 was 542 GW_{th}, which corresponds to 774 million square meters of solar collectors that represent an increment of 19 GW_{th} or 27.1 million surface area [VI]. Most of these plants employ solar heaters of the PTC type (parabolic trough collectors) [VII], as in 2022, 90 % of these solar plants used this technology [VIII]. These devices can be applied in a temperature range between 50 and 400 °C [IX].

Given the great diversity and wide application spectrum of the PTC technology, the development of theoretical models to predict its performance is paramount. Diverse models have been published in the open literature, some of them employ commercial simulation tools for its solution, while other models have been solved using other type of codes. Zima et al. [X] developed a one-dimensional model to simulate the transient performance of a PTC with a U tube for the residential sector. The model was successfully compared with a three-dimensional model coded in Ansys Fluent CFD and with experimental data.

Behar *et al*. [XI], developed a steady state model and its results were compared with experimental data achieving a close fit with an uncertainty of 0.64 %. Ferchichi *et al*. [XII] proposed a discretised model for the prediction of phase change and heat transfer for a steam generation system (DSG - Direct Steam Generation) that operates with PTC. The code was written in C^{++}. Xu et. al. [VII], established and validated a one-dimensional transient model and carried out a parametric study considering the inlet temperature of the working fluid (HTF), ambient conditions and optical efficiency. Mouaky *et al*. [XIII], simulated a four-module PTC developed by Soltigua using the Ebsilon® Professional platform. The model was validated using operating data under clear sky conditions with a maximum deviation of 4.8 %. Krishna *et al*. [XIV], employed the TRNSYS platform to simulate a phase change domestic solar PTC heater to predict the availability of hot water during the peak demand of hot water in Mangalore, India. They concluded that the system could meet the thermal duty.

From the previous review it can be observed that the steady state and transient models reproduce in a satisfactory manner the performance of PTC devices. The transient model, however, bears greater advantages in terms of control despite the highest computational needs. Additionally, all these models have been validated using fix ambient conditions within three and four consecutive days. Such experimentation does not cover the totality of seasonal and daily conditions. In this work a new one-dimensional transient model is proposed and is validated against experimental data reported in the open literature. The model was analysed under diverse seasonal and daily ambient conditions. The economic viability of a solar thermal plant using PTC technology is assessed using the pumping costs and the net present value of the life cycle energy savings.

Methodology

The transient state energy equation and the rest of the expressions that make up the model based on the representation of the phenomenon schematised in Figure 1 are presented below:

$$\frac{dQ}{dt} = F_R[G_{BH}\eta_0 A_a - A_r U_L(T_i - T_a)] \quad (1)$$

$$\frac{A_a}{A_r} = \frac{1}{\pi sin(\theta_m)} = C \quad (2)$$

ISSN 2523-2881

$$U_L = \left[\frac{A_r}{(h_{fi} + h_{r,c-a})A_a} + \frac{1}{h_{r,p-c}}\right]^{-1} \quad (3)$$

$$h_{r,c-a} = 4\sigma\varepsilon_g T_g^3 \quad (4)$$

$$h_{r,p-c} = \frac{\sigma(T_p - T_g)(T_p^2 + T_g^2)}{\left(\frac{1}{\varepsilon_p}\right) + \left(\frac{1}{\varepsilon_c} - 1\right)\left(\frac{A_r}{A_a}\right)} \quad (5)$$

$$F_r = \frac{\dot{m}c_p}{A_r U_L}\left[1 - exp\left(-\frac{U_L F' A_r}{\dot{m}c_p}\right)\right] \quad (6)$$

$$F' = \frac{\frac{1}{U_L}}{\frac{1}{U_L} + \frac{D_0}{h_w D_i} + \left[\frac{D_0}{2k_r} ln\left(\frac{D_0}{D_i}\right)\right]} \quad (7)$$

$$D_0 = 2r_r sin(\theta_m) \quad (8)$$

$$r_r = \frac{2f}{1 + cos(\varphi_r)} \quad (9)$$

$$Q = \dot{m}c_p(T_0 - T_i) \quad (10)$$

$$A_g(h_{r,c-a} + h_{c,c-a})(T_g - T_a) - A_r h_{r,p-c}(T_p - T_g) = 0 \quad (11)$$

$$T_p = \frac{Q}{h_w \pi D_i L} + T_f \quad (12)$$

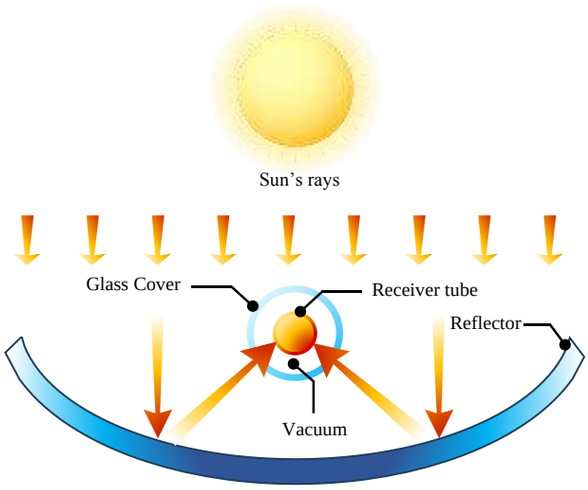

Figure 1 Schematic representation of a Parabolic Through Solar Collector

Where G_{BH} is the direct solar radiation, A_a and A_r are the aperture area and the receiver area, respectively; Q is the heat gained by the heat transfer fluid (HTF); F_R removal factor; U_L global coefficient of losses; $\theta_m$is the mean acceptance angle; T_i , T_0 and T_a are the inlet and outlet temperatures of the receiving tube, and the ambient temperature, respectively; F' the thermal efficiency factor; D_i and D_0 are the internal and external diameter of the receiving tube; $\dot{m}$ and $c_p$are the mass flow and heat capacity of the HTF; C is the solar concentration factor; f is the parabola focal length; h_w, $h_{r,c-a}$ and $h_{r,p-c}$ are the convective heat transfer coefficient of the HTF, the radiation from the glass cover to the environment, and the radiation from the receiver tube to the glass cover, respectively; r_r is the radius of the tube; and φ_r is the diffuse angle.

The transient energy balance is numerically solved using Butcher's fifth order Runge-Kutta methodology [XV]. The irradiance data used was obtained from the McClear model validated with experimental data. McClear is a clear-sky radiation model developed in the Copernicus program by the ECMWF - European Centre for Medium-Range Weather Forecasts -, which conducts non-profit research [XVI]. The environmental data of irradiance, ambient temperature, daily and seasonal wind speed was collected for the city of Guanajuato (21.0190° N, 101.2574° W) at the facilities of the University of Guanajuato, Mexico. The incidence angle of the solar rays (θ_B), and the optical efficiency, η_0 are calculated from the following expressions:

$$\eta_0 = \rho_0 \tau_g \alpha_r \gamma \left[\left(1 - A_f tan(\theta_B) cos(\theta_B)\right)\right] \quad (13)$$

$$\cos(\theta_B) = \sqrt{1 - cos^2(\delta) sin^2(h)} \quad (14)$$

Where δ is the declination angle, h is the hour angle, α_r is the receiver absorbance, τ_g is the transmittance of the tube envelope, and A_f is a geometric factor. A model code was written using the Matlab platform. Unlike the other models reported in the literature in which the equation system that makes up the model is solved simultaneously by means of an algorithm already implemented as a module, the new solution procedure is characterized by its sequential approach, which facilitates the follow-up of variables and allows control over the solution due to their high non-linearity that leads to more than one possible solution.

ISSN 2523-2881

It includes the determination of the outlet temperature and that of the glass envelope by means of the false rule method [XV], which ensures finding the correct value. Figure 2 shows the flow diagram for the solution of the model.

To ensure that the design is economically feasible, the proposed model was complemented with the *Present value of the Life Cycle Energy Savings* (PVLCES). Life Cycle Energy Savings Analysis is the difference between the life cycle cost of a system that provides an energy demand using conventional fossil energy and the life cycle cost of a solar system that provides the same energy load. The life cycle savings determine the net present value of the gain of the solar system compared to that of the conventional system [IX].

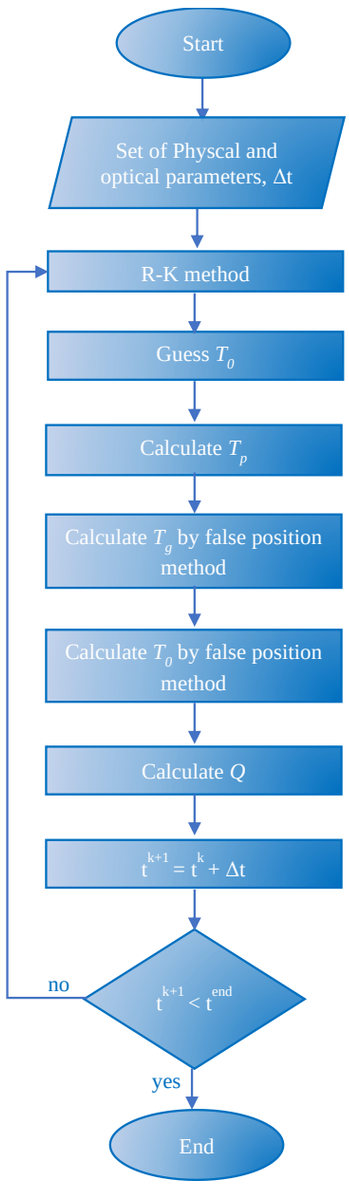

Figure 2 Flow diagram for the solution of the PTC model

The methodology reported in [XVII] was used to calculate the life cycle savings. The lifetime of the considered equipment was 25 years. Equation (15) is a general expression of economic analysis in which each of the components is calculated considering the time value of money.

$$Solar\ system\ savings = Fuel\ savings - loan\ payment - Maintaenance\ costs - insurance\ payment - Auxiliary\ energy\ costs - taxes \quad (15)$$

where,

$$Fuel\ savings = Solar\ fraction \cdot cost\ of\ fuel \cdot heat\ load \quad (16)$$

The system has a higher economic feasibility as the value of the life cycle savings increases. This analysis includes the thermal efficiency of the solar system which is represented in the economic savings of fossil fuel. On the other hand, it contemplates investment expenses, loans, taxes, operating costs (including pumping), fixed and variable maintenance in a defined time horizon.

Results

The validation of the model is done by the comparison with the experimental data reported by the Sandia National Laboratory (SNL) [XVII]. The experimental data was obtained for collectors operating with vacuum in the space of the glass envelope. The experimental tests were applied to the LS-2 solar collector installed on the AZTRAK platform at the SNL facilities. The dimensions of the system are presented in Table 1. These tests were carried out in a temperature range between 100 °C to 400 °C using water and Syltherm 800 as working fluids.

The comparative variation of the efficiency and thermal losses of the collector are presented in Figures 3 and 4. It is observed that the thermal efficiency decreases with respect to the temperature, contrary to the behaviour of the thermal losses. With the proposed model, a root mean square error (RMSE) of 1.39 °C is obtained in the prediction of the outlet temperature, with an average error of 0.24 %. For comparison purposes, Table 2 shows the mean square error of the efficiency and thermal losses calculated with other theoretical models reported in the literature.

ISSN 2523-2881

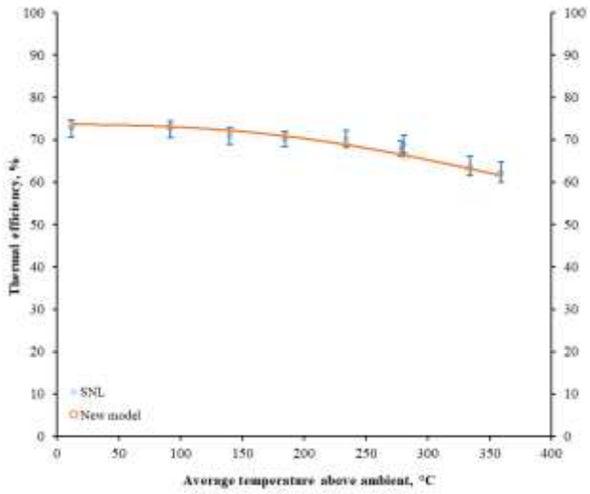

Figure 3 Comparison of the thermal efficiency calculated with the new model and the experimental data reported by SNL.

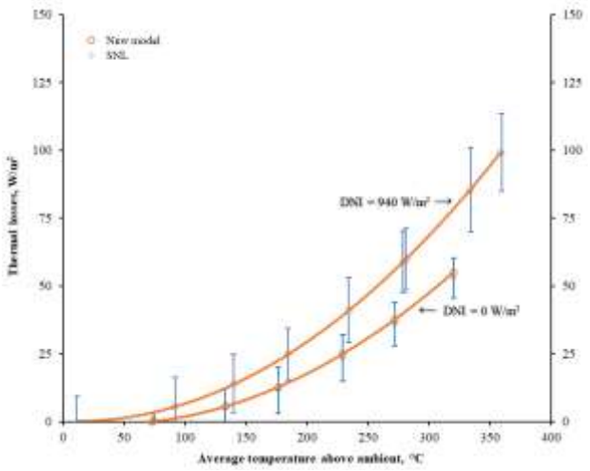

Figure 4 Comparison of thermal losses calculated with the new model and those reported by SNL.

Dimensions	Value, m
Aperture width	5
Length	7.8
Focal distance	1.84
Receiver tube inner diameter	0.066
Receiver tube outer diameter	0.07
Glass cover inner diameter	0.109
Glass cover outer diameter	0.115

Table 1 Dimensions of PTC LS-2 tested in SNL.

An analysis of the temperature and useful heat for commercial PTC dimensions [XVIII] was carried out assuming average winter and summer days of the city of Guanajuato, Mexico. The HTF used is Syltherm 800.

Model	η_t (%)	Thermal losses (W/m^2)
New model	1.019	0.368
Yilmaz and Söylemez [XIX]	0.766	4.638
Padilla *et al*. [XX]	1.012	10.255
NREL [XX1]	1.382	14.718
García-Valladares and Velázquez [XXII]	1.433	--

Table 2 RMSE comparison with some reported models.

Figures 5 and 6 show temperature and heat load profiles assuming working fluid inlet temperature in the range of 30 to 110 °C.

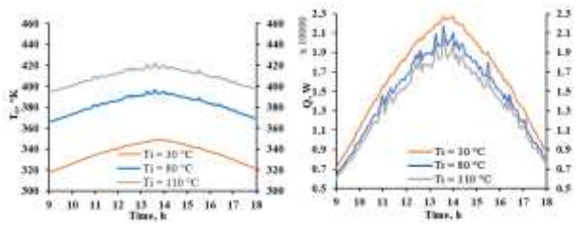

Figure 5 Temperature and heat load profile for a range of inlet temperatures (T_i) and mass flow rate $\dot{m}$ = 0.30 kg/s for a typical day in summer

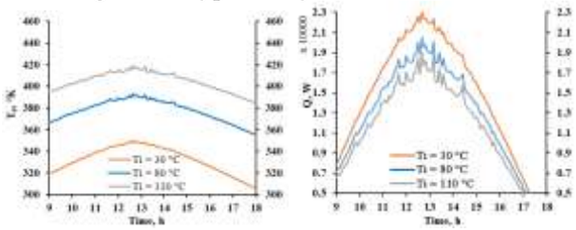

Figure 6 Temperature and heat load profile for a range of inlet temperatures (T_i) and mass flow rate $\dot{m}$ = 0.30 kg/s for a typical day in winter

Figure 7 illustrates the effect of the working fluid inlet temperature on the integrated heat of the PTC device.

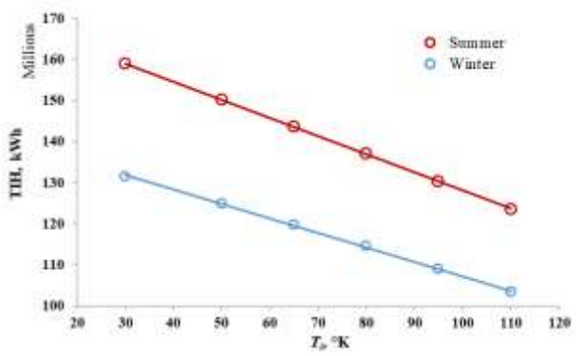

Figure 7 Effect of inlet temperature, T_i, on the total integrated heat for typical days in summer and winter and mass flow rate $\dot{m}$ = 0.30 kg/s

ISSN 2523-2881

Figure 7 shows the reduction of the integrated useful heat with the increment of inlet temperature of the HTF. The data shows a linear profile. The model provides the temperature and integrated heat load for any set of ambient conditions.

The variation of the mass flow rate between 0.3 and 0.6 kg/s and its effect on outlet temperature and heat load is depicted in Figures 8 and 9 for typical days in summer and winter. In these calculations, the inlet temperature was kept at 80 °C.

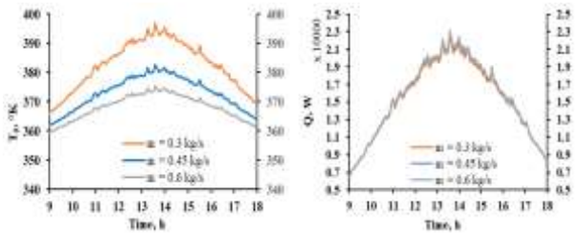

Figure 8 Effect of mass flow, $\dot{m}$, on outlet temperature, T_0, and thermal load, Q. T_i= 80 °C. Typical day of summer

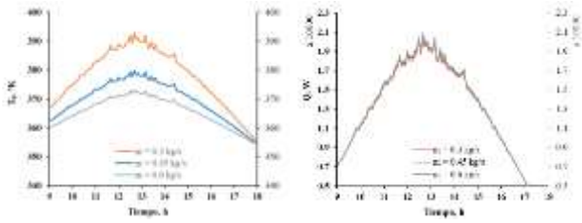

Figure 9 Temperature and heat load profile for different mass flow rates and T_i = 80 °C. Typical day in Winter

Figure 10 shows the effect of the mass flow rate on the integrated heat. A parametric study was also performed to analyse the effect of the design variables on the PTC using the *Present value of the Life Cycle Energy Savings* (PVLCES) and the integrated useful heat (TIH). This indicator is the integration of the instantaneous heat gained by the HTF between 9:00 and 18: 00 h:

$$TIH = Total\ Integrated\ Heat = \int_{t=9\ h}^{t=18\ h} q_t \qquad (17)$$

Where q_t is the instantaneous heat gained by the HTF.

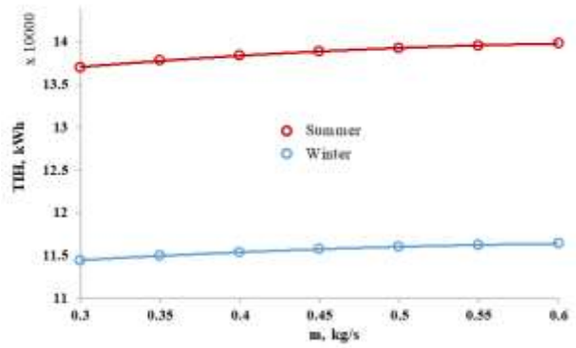

Figure 10 Effect of mass flow rate on the total integrated useful heat for typical days in summer and winter and T_i = 80 °C

The parametric study is carried out considering the following design variables: length, collector aperture, focal length, inner diameter of the receiver tube and inner diameter of the transparent glass cover (Table 3). Additionally, four different heat transfer fluids were analysed: Dowtherm A, Syltherm 800, Therminol VP-1, and pressurised water. The range of variation of each of the variables was taken from the data reported in the open literature for commercial collectors [XXIII].

Dimension, m	LB	UB
L	2	25
W_a	0.5	9.3
f	0.2	3
D_i	0.01	0.04
Dg_i	0.11	0.15

Table 3 Variables range on the parametric analysis

Figure 11 shows the variation of the PVLCES and the total integrated heat with the length, L. It can be observed that the PVLCES becomes negative for some values of L. On the other hand, as the length increases, the total integrated heat increases in a linear manner.

The effect of the variation of the aperture, W_a, is depicted in Figure 12. It can be observed that there is an optimum where both the PVLCES and the total integrated heat are maximised.

ISSN 2523-2881

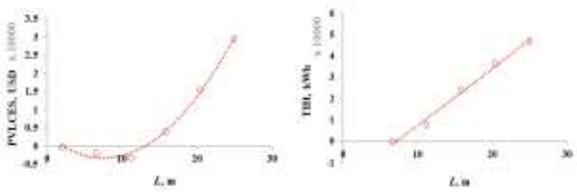

Figure 11 Effect of length, **L**, on the PVLCES and total integrated heat for a typical day in summer

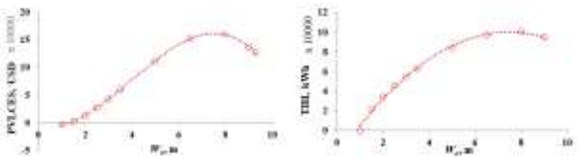

Figure 12 Effect of the aperture on the PVLCES and total integrated heat for a typical day in summer

The effect of the focal length, ***f***, is shown in Figure 13. The profiles indicate that after certain value of ***f***, the increment of this variable has minimal effect of PVLCES and total integrated heat.

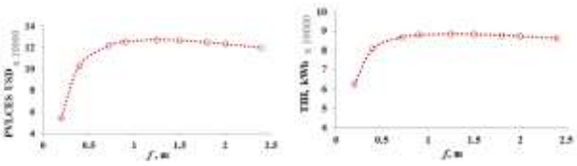

Figure 13 Effect of the focal length on PVLCES and total integrated heat for a typical day in summer

The variation of the inner diameter of the receiver tube, D_i, and the glass cover, Dg_i, is displayed in Figures 14 and 15 respectively.

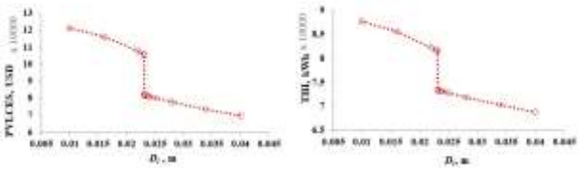

Figure 14 Effect of the inner diameter of the receiver tube, D_i, on the PVLCES and the total integrated heat for a typical day in summer

For the inner diameter of the receiver tube, it is observed that at certain value the PVLCES and total integrated heat drop drastically ($D_i \approx 0.023$ m). On the other hand, the variation of the inner diameter of the glass cover does not affect significantly any of the parameters.

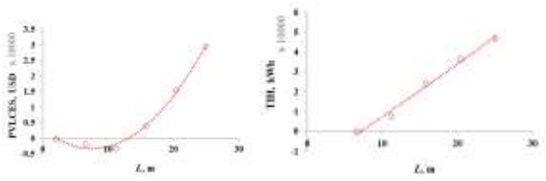

Figure 15 Effect of the inner diameter of the glass cover, Dg_i on the PVLCES and total integrated heat for a typical day in summer

Finally, Figure 16 shows the effect of the type of working fluid on the parameters.

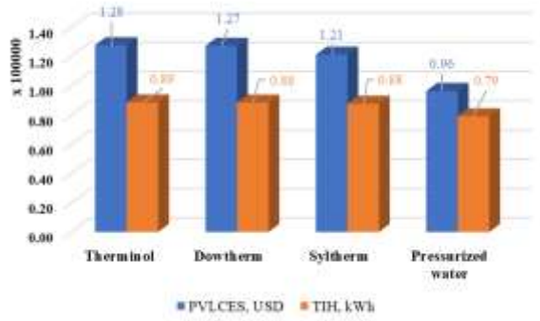

Figure 16 Effect of the type of working fluid on PVLCES and total integrated heat for a typical day in summer

In this study, the working fluid for which the highest performance is obtained is Therminol followed by Dowtherm. The performance with the different thermal oils is similar while the use of pressurised water renders the lowest performance.

Conclusions

Form the results obtained, the following conclusions are drawn:

1. Due to the high non-linearity of the thermal model, the sequential solution approach ensures that the correct solution is found.

2. The thermal model was validated against experimental data and statistical indicators reported by other models in the open literature. This ensures the reliability of the new model.

3. The present value of the life cycle energy savings (PVLCES) is a useful parameter that allows to determine the economic feasibility of the installation of a solar thermal plant.

ISSN 2523-2881

4. From the parametric analysis it can be concluded that the diameter of the cover glass is the design variable has the minimal impact on the economic performance and total heat recovered. On the contrary, the length and PTC width are the variables that bear the strongest influence.

5. The inner diameter of the receiver tube favours the thermal efficiency. At lower dimensions the Re number increases and the heat transfer capacity as well. The analysis of this variable exhibits an abrupt discontinuity which increases the complexity of the solution.

6. Amidst the working fluids, the thermal oils have similar high performance but are much higher than that obtained with pressurised water.

7. The new thermal model is suitable to be used in optimisation and control studies due to its transient nature.

8. Future work underway is the design optimisation of PTC for industrial applications. A metaheuristic algorithm is proposed given the high nonlinearity of the system and the apparent discontinuity of the performance with the inner diameter of the receiver tube.

Acknowledgments

Juan Ramón Lizárraga Morazán is grateful to CONAHCyT and the Department of Chemical Engineering of the Division of Natural and Exact Sciences of the University of Guanajuato, for the support in the development of this research.

References

[I] Philibert, C. Insight Series. 2017.

[II] Birol, F. World Energy Investment. 2023, 1–183.

[III] Pramanik, S.; Ravikrishna, R. V. A Review of Concentrated Solar Power Hybrid Technologies. Appl Therm Eng 2017, 127, 602–637, doi:10.1016/j.applthermaleng.2017.08.038.

[IV] Awan, A.B. Comparative Analysis of 100 MW Concentrated Solar Power Plant and Photovoltaic Plant. AIP Conf Proc 2019, 2119, doi:10.1063/1.5115363.

[V] Salgado Conrado, L.; Rodriguez-Pulido, A.; Calderón, G. Thermal Performance of Parabolic Trough Solar Collectors. Renewable and Sustainable Energy Reviews 2017, 67, 1345–1359, doi:10.1016/j.rser.2016.09.071.

[VI] Spork-Dur, W. Solar Heat World Wide. 2022, 88; https://www.iea-shc.org/Data/Sites/1/publications/Solar-Heat-Worldwide-2022.pdf. Acceso: 10 julio 2023.

[VII] Xu, L.; Sun, F.; Ma, L.; Li, X.; Lei, D.; Yuan, G.; Zhu, H.; Zhang, Q.; Xu, E.; Wang, Z. Analysis of Optical and Thermal Factors' Effects on the Transient Performance of Parabolic Trough Solar Collectors. Solar Energy 2019, 179, 195–209, doi: 10.1016/j.solener.2018.12.070.

[VIII] Adib, R.; Zervos, A. Renewables 2023 Global Status Report; 2023; https://www.ren21.net/wp-content/uploads/2019/05/GSR2023_Demand_Modules.pdf. Acceso: 9 julio 2023.

[IX] Kalogirou, S. Solar Energy Engineering. [Electronic Resource] : Processes and Systems. 2009.

[X] Zima, W.; Cebula, A.; Cisek, P. Mathematical Model of a Sun-Tracked Parabolic Trough Collector and Its Verification. Energies (Basel) 2020, 13, doi:10.3390/en13164168.

[XI] Behar, O.; Khellaf, A.; Mohammedi, K. A Novel Parabolic Trough Solar Collector Model - Validation with Experimental Data and Comparison to Engineering Equation Solver (EES). Energy Convers Manag 2015, 106, 268–281, doi: 10.1016/j.enconman.2015.09.045.

[XII] Ferchichi, S.; Kessentini, H.; Morales-Ruiz, S.; Rigola, J.; Bouden, C.; Oliva, A. Thermal and Fluid Dynamic Analysis of Direct Steam Generation Parabolic Trough Collectors. Energy Convers Manag 2019, 196, 467–483, doi:10.1016/j.enconman.2019.05.107.

[XIII] Mouaky, A.; Alami Merrouni, A.; Laadel, N.E.; Bennouna, E.G. Simulation and Experimental Validation of a Parabolic Trough Plant for Solar Thermal Applications under the Semi-Arid Climate Conditions. Solar Energy 2019, 194, 969–985, doi:10.1016/j.solener.2019.11.040.

[XIV] Krishna, Y.; Faizal, M.; Saidur, R.; Manihalla, P.P.; Karinka, S. Performance Analysis of Parabolic Trough Collector Using TRNSYS®-A Case Study in Indian Coastal Region. J Phys Conf Ser 2021, 1921, doi:10.1088/1742-6596/1921/1/012063.

[XV] Chapra, S.C. Applied Numerical Methods With Matlab® For Engineers And Scientists; McGrawHill Education, Ed.; 4th ed.; New York, 2018.

[XVI] ECMWF Copernicus, Atmosphere Monitoring Service Available online: https://atmosphere.copernicus.eu/, acceso: 2 junio 2023.

[XVII] Caballero-Esparza, M.; Lizárraga-Morazán, J.R.; Picón-Núñez, M. Economic Analysis for the Selection of Low Temperature Solar Thermal Utility Systems. Appl Therm Eng 2022, 215, 118913, doi: 10.1016/j.applthermaleng.2022.118913.

[XVIII] Dudley, E.; Kolb, J.; Mahoney, A.; Mancini, T.; M, S.; Kearney, D. Test Results: SEGS LS-2 Solar Collector. Sandia National Laboratory. Report: SAND94- 1884. 1994, 140.

[XIX] Yilmaz, I.H.; Söylemez, M.S. Thermo-Mathematical Modeling of Parabolic Trough Collector. Energy Convers Manag 2014, 88, 768–784, doi: 10.1016/J.ENCONMAN.2014.09.031.

[XX] Padilla, R.V.; Demirkaya, G.; Goswami, D.Y.; Stefanakos, E.; Rahman, M.M. Heat Transfer Analysis of Parabolic Trough Solar Receiver. Appl Energy 2011, 88, 5097–5110, doi: 10.1016/J.APENERGY.2011.07.012.

[XXI]Forristall, R. Heat Transfer Analysis and Modeling of a Parabolic Trough Solar Receiver Implemented in Engineering Equation Solver; Golden, CO (United States), 2003.

[XXII] García-Valladares, O.; Velázquez, N. Numerical Simulation of Parabolic Trough Solar Collector: Improvement Using Counter Flow Concentric Circular Heat Exchangers. Int J Heat Mass Transf 2009, 52, 597–609, doi: 10.1016/J.IJHEATMASSTRANSFER.2008.08.004.

[XXIII] Meyers; R.A. Encyclopedia of Sustainability Science and Technology 2013, 7619–7622.

ISSN 2523-2881

Article **Journal Renewable Energy**
December, 2023 Vol.7 No.19 28-37

Geothermal energy harnessing using a horizontal composite geothermal heat exchanger and a vertical geothermal heat exchanger

Aprovechamiento de la energía geotérmica utilizando un intercambiador de calor geotérmico compuesto horizontal y un intercambiador de calor geotérmico vertical

RUBIO-LÓPEZ, Osvaldo†*, MONTOYA-SANTIYANES, Luis Alvaro, GARCÍA-GUENDULAIN, Juan Manuel and MENDOZA-ROJAS, América Eileen

Universidad Politécnica de Querétaro, El Marques, Queretaro 76240, Mexico

ID 1st Author: *Osvaldo, Rubio-López* / **ORC ID**: 0000-0002-9073-8249, **CVU CONAHCYT ID**: 484537

ID 1st Co-author: *Luis Alvaro, Montoya-Santiyanes* / **ORC ID**: 0000-0003-3380-1544, **CVU CONAHCYT ID**: 492895

ID 2nd Co-author: *Juan Manuel, García-Guendulain* / **ORC ID**: 0000-0001-5636-5074, **CVU CONAHCYT ID**: 514795

ID 3rd Co-author: *América Eileen, Mendoza-Rojas* / **ORC ID**: 0000-0003-5636-5074, **CVU CONAHCYT ID**: 854644

DOI: 10.35429/JRE.2023.19.7.28.37 Received July 03, 2023; Accepted November 30, 2023

Abstract

Heat exchangers in combination with geothermal heat pumps (GHP) have been growing in HVAC and sanitary applications, as well as associated research. Therefore, in this work, a Composite Geothermal Heat Exchanger (CGHE) and a Horizontal Geothermal Heat Exchanger (HGHE) were designed and fabricated Through experimental tests and simulation in ANSYS-CFX, the behavior of the temperature of the refrigerant fluid inside the exchangers was compared. The geometry of the CGHE was based on a Vertical Geothermal Heat Exchanger (VGHE) with the installation depth of an HGHE. Water at different temperatures was used as the cooling fluid with a mass flow equal to 0.26 L/s for the experimental tests and simulations in ANSYS-FLUENT for both the CGHE and HGHE. The CGHE and HGHE were installed within a volume of 3.25 m^3 of ground. The experiments and simulations in ANSYS-CFX showed that the refrigerant fluid inside the CGHE exhibit a greater use of geothermal energy because it increases and reduces the temperature of the refrigerant more quickly compared to the HGHE.

Energy, Geothermal, Exchanger

Resumen

Los intercambiadores de calor en combinación con las bombas de calor geotérmicas han demostrado un crecimiento en aplicaciones sanitarias y de climatización, así como investigaciones asociadas. Por lo tanto, en este trabajo se diseñó y construyó un Intercambiador de Calor Geotérmico Compuesto (ICGC) y un Intercambiador de Calor Geotérmico Horizontal (ICGH). A través de pruebas experimentales y simulación en ANSYS-CFX se comparó el comportamiento de la temperatura del fluido refrigerante en el interior de los intercambiadores. La geometría del ICGC fue basada en un Intercambiador de Calor Geotérmico Vertical (ICGV) con la profundidad de instalación de un ICGH. Se utilizó agua como refrigerante variando la temperatura, y un flujo másico igual a 0.26 L/s fue utilizado tanto en los experimentos como en las simulaciones para ambos intercambiadores. El ICGC y el ICGH fueron instalados dentro de un volumen de 3.25 m^3 de tierra. Los experimentos y la simulación en ANSYS-CFX mostraron que el fluido refrigerante dentro del ICGC presenta un aprovechamiento mayor de la energía geotérmica debido a que incrementa y reduce más rápido la temperatura del fluido refrigerante en comparación al ICGH.

Energía, Geotermia, Intercambiador

Citation: RUBIO-LÓPEZ, Osvaldo, MONTOYA-SANTIYANES, Luis Alvaro, GARCÍA-GUENDULAIN, Juan Manuel and MENDOZA-ROJAS, América Eileen. Geothermal energy harnessing using a horizontal composite geothermal heat exchanger and a vertical geothermal heat exchanger. Journal Renewable Energy. 2023. 7-18: 28-37

* Author Correspondence (e-mail: osvaldo.rubio@upq.edu.mx)
† Researcher contributing as first author.

1. Introduction

A Geothermal Heat Pump (GHP) extracts the thermal energy from underground by means of a Geothermal Heat Exchanger (GHE), and through that energy supply evaporates a cooling fluid at very low pressure and temperature that is compressed through a compressor, thus increasing its temperature and pressure. The steam then passes to the condenser and gives heat to the medium to heat. Finally, the fluid passes through an expansion valve, reducing its temperature and pressure again and restarting the refrigeration cycle (Mustafa, 2008).

This provides significant energy savings of between 30% and 70% compared to conventional cooling and heating systems (Benli & Durmus, 2009). Heat exchangers hold a pivotal role in process production, chiefly segmented into four groups based on heat transfer principles (Gong *et al*., 2023) direct contact heat exchangers (Zheng *et al*., 2022), accumulator heat exchangers (Chen *et al.*, 2022) surface heat exchangers (Triki *et al*., 2021), and inter-wall heat exchangers (Guo *et al*., 2014), with the latter being most prevalent in industrial use and having received comprehensive examination (Lv *et al.*, 2018).

The first known records that are held in using the land as a heat source using a GHP is a Swiss patent issued and registered in the year 1912 (Philippe *et al*., 2011) However, with the development of the classical heat conduction theory (ground-pipe) proposed by Ingersoll and Plass in 1948, as well as the analytical basic theory for heat conduction in GHP systems also proposed by Ingersoll and Plass (Ingersoll *et al*., 1950; Rousseau *et al*., 2017).

Over the past two decades, major efforts have been made to establish standards for the installation and development of GHE design methods by the International Geothermal Ground Source Heat Pump Association (IGSHPA, 2013; Eskilson, 1987; Rees, 2016; IGSHPA, 2018). It is estimated that GHP's facilities have grown continuously worldwide, with an annual interval between 10% and 30% in recent years (Fundación de la Energía de la Comunidad de Madrid, 2010).

GHEs make use of geothermal energy stored in the subsoil, classified as energy at very low temperature (T<30ºC), this energy can be used for heating, air conditioning and domestic hot water, making use of a GHP (Bose et al., 1985). (Yang *et al*., 2009) VGHEs have a geometric configuration in U or double U, with an internal diameter pipe that ranges between 19 mm and 38 mm, and each borehole for the installation of the VGHE has a depth ranging from 20 m to 200 m with a diameter ranging from 100 mm to 200 mm (Philippe *et al*., 2011).

To perform these functions, the GHP uses an HGHE and a VGHE, see Figure 1a and 1b (Mustafa *et al*., 2008; IGSHPA, 2018).

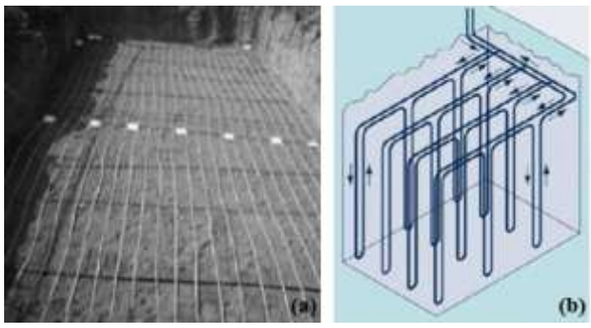

Figure 1 An HGHE installed in the subsoil at a depth of 2 meters
Huseyin Benli[a], Aydın Durmus[b], 2008

The article is mainly structured as follows: Section 2 shows the methodologies used to estimate the lengths of the exchangers and the selection of subsoil temperatures at different depths. In Section 3, the experiments and numerical simulations carried out to find the temperature distributions are specified. Section 4 specifies discussions and conclusions.

2. Metodology

2.1. Calculation of CGHE and HGHE lengths

The Composite Geothermal Heat Exchanger (CGHE) and HGHE of 15.8 m length with PEAD4710 high density polyethylene pipe were designed and built. CGHE and HGHE were installed in a subsoil external control volume equal to 3.25 m^3 of ground (see Figure 2) and in a subsoil control volume equal to 3.25 m^3 of ground (see Figure 3). The CGHE combines the geometry of a VGHE and the installation depths of a HGHE.

ISSN 2523-2881

The temperature behavior of the refrigerant fluid that circulates inside the GHEs was studied through six experimental tests and simulations in the ANSYS-FLUENT software, where water is considered as the refrigerant fluid subjected to different working temperatures.

The lengths for the CGHE and HGHE geometries was calculated according to the IGSHPA. The model established by the IGSHPA (IGSHPA, 2009) is based on Kelvin's linear heat source theory with some simplified assumptions. By using this method and the Equation (1), the total lengths are calculated considering the month with the lowest temperature recorded in the city of Santiago de Queretaro, Mexico, 2021.

$$L_H = \frac{Capacity_C\left(\frac{COP_C+1}{COP_C}\right)(R_P+R_S \cdot F_H)}{T_{max}-T_{s,m}} \quad (1)$$

where R_s represents the thermal resistance of the ground which is taken from Table 1, referring to a Vertisol type soil (National Institute of Geographical and Informatics Statistics, INEGI 2007), R_p is the thermal resistance of the pipe from CGHE and HGHE, F_H is the GHP operating factor, $Capacity_C$ is the refrigeration capacity, $T_{s,m}$, is the average temperature of the ground at a set depth, and T_{max} is the maximum temperature at the inlet of the refrigerant fluid to the GHP.

By substituting the values of the variables in Equation (1), the total length for the CGHE and HGHE is obtained, $L_H = 15.75\, m$ which turned out to be the same for both models.

The experiments were carried out at the CGHE and HGHE under two different boundary conditions. Figure 2 shows the first boundary condition, at which the external volume to the subsoil equal to 3.25 m^3 was fabricated and that is where the models were installed to perform the tests with water as refrigerant at different working temperatures.

Figure 2 First boundary condition with the external volume to the subsoil

For the second boundary condition, the same volume of 3.25 m^3 was considered but now excavated underground, and in this excavation the CGHE and HGHE were installed. The same experimental tests considering water as a refrigerant at different temperatures were carried out (see Figure 3).

Figure 3 Second boundary condition with the volume excavated in the subsoil

In the experimental tests, the next parameters were monitored for the refrigerant fluid: outlet speed, the temperatures at the inlet and outlet, and mass flow. The mass flow was used to estimate pressure losses within the geometry of the CGHE and HGHE.

Figure 4 shows the geometry of the CGHE with the length of 15.8 m according to the results obtained with Equation 1.

ISSN 2523-2881

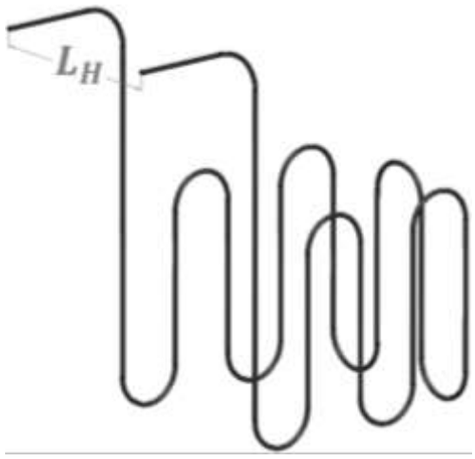

Figure 4 CGHE geometry

Figure 5 shows the geometry of the HGHE with the length of 15.8 m according to the results obtained with Equation 1.

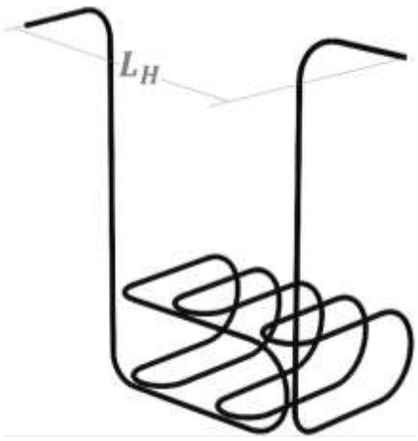

Figure 5 HGHE geometry

According to data from National Institute of Geographical and Informatics Statistics (INEGI, 2007; Consejo de Ciencia y Tecnología del Estado de Querétaro [CONCYTEQ], 2002) topographic data from the city of Santiago de Queretaro, Mexico, it is shown that Vertisol-type soils predominate, a soil with a high clay content classified as red or pottery clay and as light or semi-dry soil (INEGI, 2007).

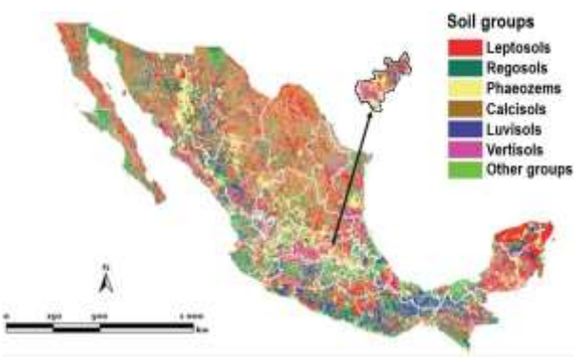

Figure 6 Classification of soil in Mexico, specifically in city of Queretaro

Table 1 contains the main thermophysical properties of Vertisol-type soil (INEGI, 2021).

Properties	Value
Thermal conductivity (λ)	0.46 W/m·ºC
Density (ρ)	2000 Kg/m^3
Specific heat (C_P)	879 J/Kg·ºC
Thermal diffusivity (α)	2.6166 x 10^{-7} m^2/s

Table 1 Thermophysical properties of a Vertisol-type soil

2.2. Temperature behavior in the city of Queretaro, Mexico

The city of Santiago de Queretaro is located at 20° 35' North latitude, with a longitude of 100° 23' West and an altitude of 1820 m s. n. m. (National Institute of Geographical and Informatics Statistics (INEGI 2007). The temperature recorded during 2021 was decisive to calculate the behavior of refrigerant fluid temperature in both models CGHE and HGHE. Graph 1 shows the behavior of the maximum, minimum and average temperatures (Meteored, 2023). (Data collected by the closest weather stations to the Queretaro International Airport (MMQT)).

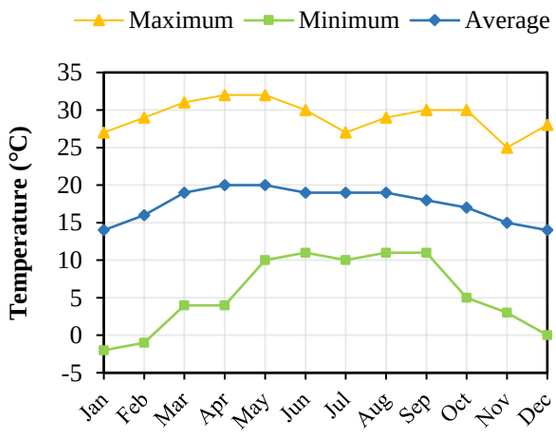

Graph 1 Behavior of maximum, minimum and average temperatures

2.3. Annual Oscillation of Surface Temperature (AOs)

The AOs is determined by using Equation 2. (Kusuda & Achenbach, 1965).

$$AOs = \left(\underset{Monthly}{Average\ Temperature}\right) - \left(\underset{Annualy}{Average\ Temperature}\right) \quad (2)$$

ISSN 2523-2881

Table 2 shows the AOs in the city of Queretaro, Mexico, corresponding to the closest meteorological temperatures to the Queretaro International Airport (MMQT).

Month	Average Temperature Monthly (°C)	Average Temperature Annually (°C)	AOs (°C)
January	14	17.362	-3.362
February	16	17.362	-1.362
March	19	17.362	1.638
April	20	17.362	2.638
May	20	17.362	2.638
June	19	17.362	1.638
July	19	17.362	1.638
August	19	17.362	1.638
September	18	17.362	0.638
October	17	17.362	-0.362
November	15	17.362	-2.362
December	14	17.362	-3.362
Average	17.362	17.362	

Table 2 Annual Oscillation of Surface Temperature.

The AOs is obtained by taking the interval between upper and lower values in Graph 2.

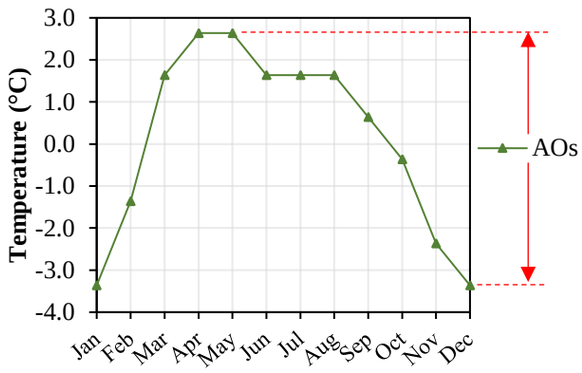

Graph 2 Overall behavior of the AOs in the city of Queretaro, Mexico

2.4. Evolution of the subsoil temperature at different depths

Considering a homogeneous and isotropic Vertisol type soil with constant thermophysical properties, the temperature at any depth Z can be calculated in a time t. Then, the internal temperature of subsoil at different depths is calculated by using Equation 3 (Kusuda & Achenbach, 1965) and data from Graph 1.

$$T(Z,t) = T_m - OA_S \cdot e^{-Z\sqrt{\frac{\pi}{365\cdot\alpha}}} cos\left[\frac{2\pi}{365}\left(t - t_0 - \frac{Z}{2}\sqrt{\frac{365}{\pi\alpha}}\right)\right] \quad (3)$$

A depth interval is selected from 0 to 6 m, and by using Table 1 values as input for Equation 3, the temperature of subsoil is calculated.

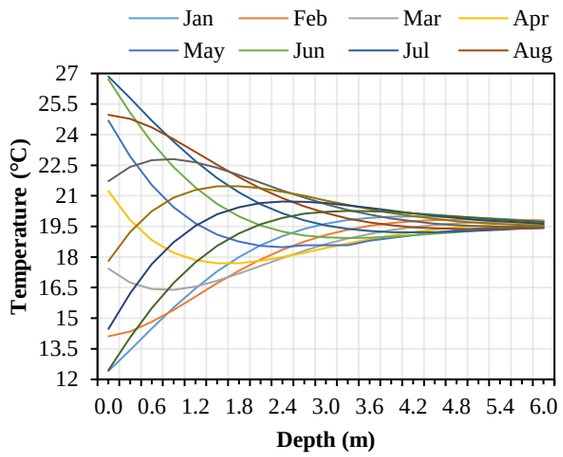

Graph 3 Behavior of internal temperature of subsoil

Graph 3 indicates there is a greater temperature difference on the ground's surface in the months of January - July (Sossa & Sebastián, 2013). and this temperature difference decreases with increasing depth in the subsoil.

3. Results

3.1. Experimental tests at the CGHE and HGHE

Five tests were carried out considering the two boundary conditions mentioned before (see Figures 2 and 3) as well as five simulations in ANSYS-FLUENT for each heat exchanger. The first and second runs were chosen to be analyzed. The first test was performed using water as a refrigerant at 7.35 °C and the second test was similar but at 60.05 °C.

Table 3 shows the temperature results of the 1st and 2nd experimental tests conducted at the CGHE and HGHE.

Test No.	Inlet Temp. (CGHE)	Outlet Temp. (CGHE)	ΔT (°C) (CGHE)
1	7.35 °C	8.62 °C	ΔT = 1.27 °C
2	60.05 °C	57.12 °C	ΔT = 2.96 °C
Test No.	**Inlet Temp. (HGHE)**	**Outlet Temp. (HGHE)**	**ΔT (°C) (HGHE)**
1	7.35 °C	7.95 °C	ΔT = 0.6 °C
2	60.05 °C	57.75 °C	ΔT = 2.24 °C

Table 3 Temperatures of the refrigerant fluid in the 1st and 2nd experimental tests

Graph 4 shows that the CGHE presents a higher ΔT than the HGHE in both tests.

ISSN 2523-2881

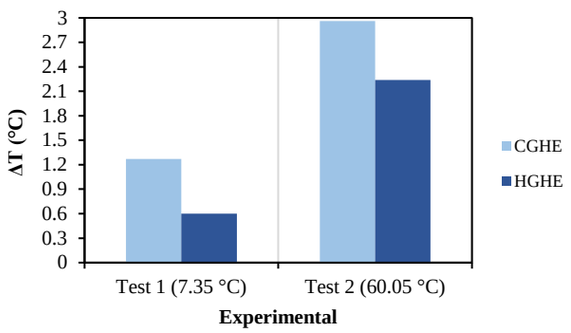

Graph 4 Comparison of experimental ΔT at the CGHE and HGHE

3.2. Boundary conditions in CFD simulations for the CGHE and for the HGHE

The boundary conditions established in the ANSYS-FLUENT simulations are described as follows and can be reviewed in the Figure 7:

- Subsoil temperature profile (Graph 3).
- Vertisol type soil thermal properties (Table 1).
- Thermal properties of PEAD4710.
- Temperature of the refrigerant fluid (water) at 7.35 °C and 60.05 °C.
- Thermophysical properties of the refrigerant fluid (water) at 7.35 °C and 60.05 °C.
- Mass flow rate of the refrigerant fluid.
- Velocity of the refrigerant fluid inside the CGHE and HGHE.

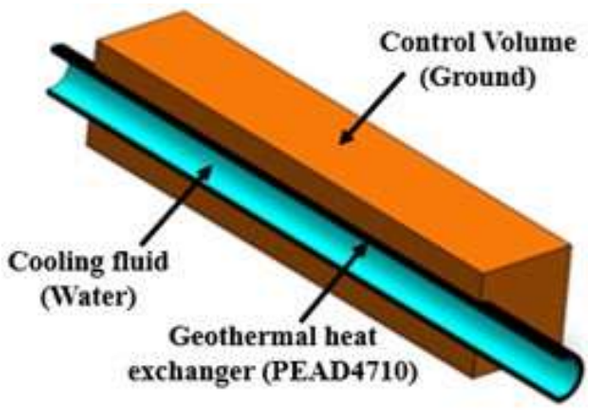

Figure 7. Cross section view of the domain used for setting the boundary conditions in Ansys for CGHE and HGHE

3.3. Results of the numerical simulation of the refrigerant fluid inside the CGHE at a temperature of 7.35 °C

Test 1 was chosen using water as a refrigerant fluid at a temperature of 7.35 °C. Figure 8 depicts the distribution of the temperature inside the CGHE.

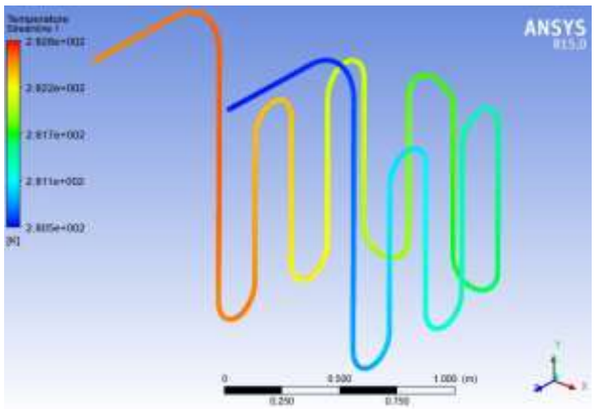

Figure 8 Temperature distribution of the refrigerant fluid inside the CGHE through test 1 at 7.35 °C

3.4. Numerical simulation of the refrigerant fluid inside the CGHE at a temperature of 60.05 °C

Test 2 was chosen using water as a refrigerant fluid at a temperature of 60.05 °C. Figure 9 depicts the distribution of the temperature inside the CGHE.

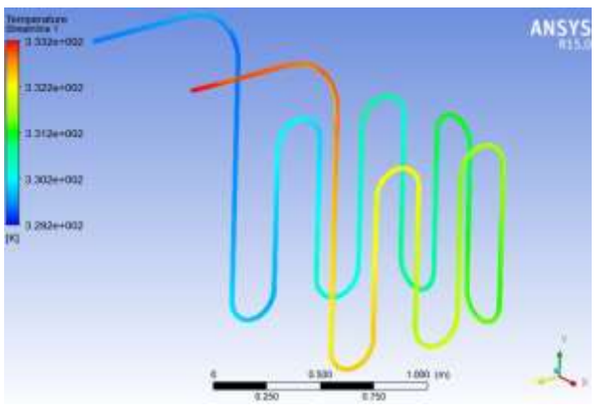

Figure 9 Temperature distribution of the refrigerant fluid inside the CGHE through test 2 at 60.05 °C

3.5. Numerical simulation of the refrigerant fluid inside the HGHE at a temperature of 7.35 °C

Test 1 was chosen using water as a refrigerant fluid at a temperature of 7.35 °C. Figure 10 depicts the distribution of the temperature inside the HGHE.

ISSN 2523-2881

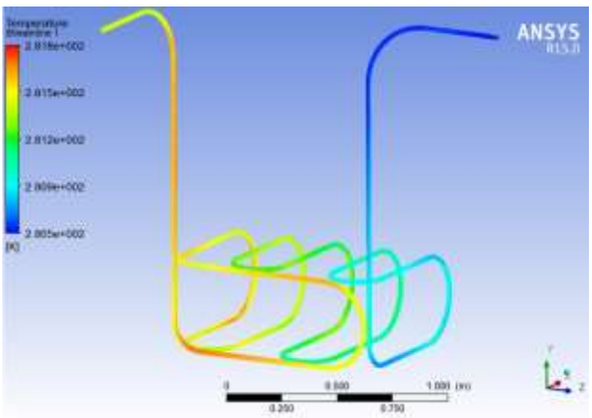

Figure 10 Temperature distribution of the refrigerant fluid inside the HGHE through test 1 at 7.35 °C.

3.6. Numerical simulation of the refrigerant fluid inside the HGHE at a temperature of 60.05 °C

Test 2 was chosen using water as a refrigerant fluid at a temperature of 60.05 °C. Figure 11 depicts the distribution of the temperature inside the HGHE.

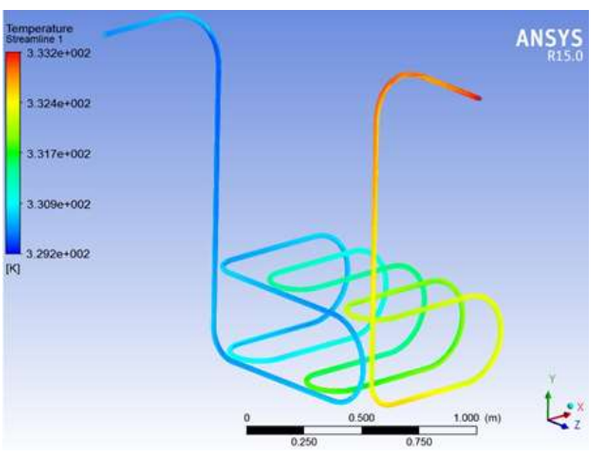

Figure 11. Temperature distribution of the refrigerant fluid inside the HGHE through test 2 at 60.05 °C.

Table 4 describes the results obtained in the ANSYS-FLUENT simulations for tests 1 and 2.

Test No.	Inlet Temp. (CGHE)	Outlet Temp. (CGHE)	ΔT (°C) (CGHE)
1	7.35 °C	9.65 °C	ΔT = 2.3 °C
2	60.05 °C	55.87 °C	ΔT = 4.18 °C
Test No.	**Inlet Temp. (HGHE)**	**Outlet Temp. (HGHE)**	**ΔT (°C) (HGHE)**
1	7.35 °C	8.65 °C	ΔT = 1.3 °C
2	60.05 °C	56.05 °C	ΔT = 4.0 °C

Table 4 Temperatures of the refrigerant fluid in the 1st and 2nd numerical tests.

Graph 5 shows that the CGHE presents a higher ΔT than HGHE just in the 1st test.

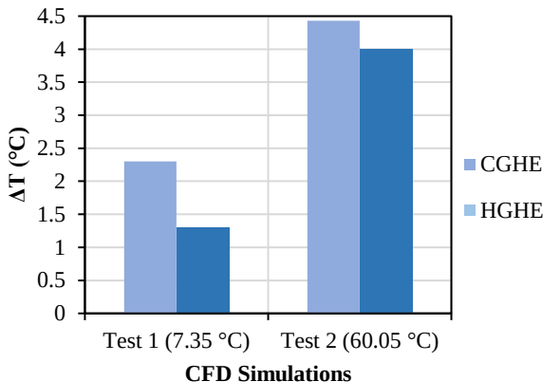

Graph 5 Comparison of numerical ΔT at the CGHE and HGHE.

3.7. Comparative analysis CGHE vs HGHE

The temperature distribution of the refrigerant fluid studied with ANSYS-FLUENT was monitored at different points of the geometry for the CGHE and HGHE for intervals of length equal to 2.25 m considering both tests 1 and 2.

Thus, Graph 6 shows the variation of temperature of the refrigerant fluid at different positions of the CGHE and HGHE geometries at an inlet temperature of 7.35 °C.

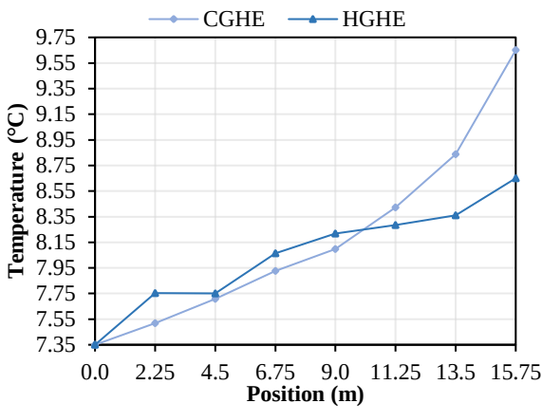

Graph 6 Comparative analysis (7.35 °C): CGHE vs HGHE.

The behavior of the temperature of the refrigerant fluid throughout the position is similar for both exchangers in terms of magnitude, however, in the final positions the CGHE exchanger is considerably separated from the HGHE, see Graph 6. These results correspond to the inlet temperature of 7.35 °C. The temperature in the CGHE is approximately linear while in the HGHE this is lost.

ISSN 2523-2881

The behavior of the temperature of the refrigerant fluid throughout the position is similar for both exchangers in terms of magnitude, however, in the final positions the HGHE exchanger is considerably separated from the CGHE, see Graph 7. These results correspond to the inlet temperature of 60.05 °C. Both exchangers behaved decreasing linearly.

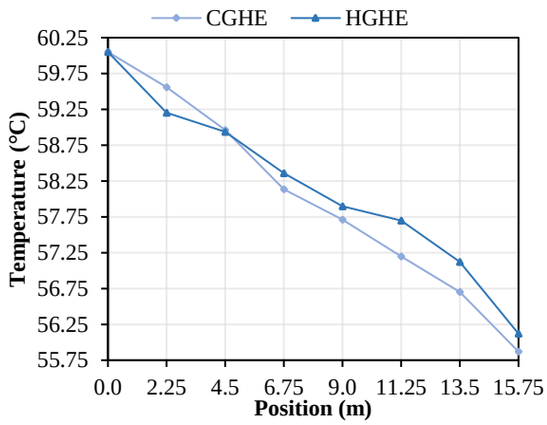

Graph 7 Comparative analysis (60.05 °C): CGHE vs HGHE.

4. Acknowledgements

The authors thank the Center for Engineering and Industrial Development (CIDESI) for the facilities provided to carry out the experimentation and the Polytechnic University of Queretaro (UPQ) for its support and funding of the work.

5. Conclusions

Based on data in Table 4 for ΔT, the following can be concluded:

1. In test 1 where the refrigerant fluid (water) had an inlet temperature of 7.35 °C, the ΔT had a 52.76% greater difference in the CGHE in relation to the HGHE.

2. In test 2 with the refrigerant (water) at the inlet at 60.05 °C, the ΔT had a 24.33% greater difference in the CGHE in relation to the HGHE.

From the experiments and the simulations in ANSYS-FLUENT for the CGHE model, the following can be concluded:

1. The results of experimental test 1 and numerical simulation 1 only presented a temperature difference equal to 1.03 °C.

2. The results of experimental test 2 and numerical simulation 2 only presented a temperature difference equal to 1.22 °C.

3. The refrigerant temperature for the CGHE model behaved practically linear in both tests, with the temperature at the inlet of the refrigerant fluid at 7.35 °C and 60.05 °C, respectively. This behavior is not observed in the same way for the HGHE model, where it was mostly non-linear.

From the experiments and the simulations in ANSYS-FLUENT for the HGHE model, the following can be concluded:

1. The results of experimental test 1 and numerical simulation 1 only presented a temperature difference equal to 0.7 °C.

2. The results of experimental test 2 and numerical simulation 2 only presented a temperature difference equal to 1.76 °C.

6. References

Benli, H. & Durmus, A. (2009). Evaluation of ground-source heat pump combined latent heat storage system performance in greenhouse heating. *Energy and Buildings*, 41(2), 220-228. https://doi.org/10.1016/j.enbuild.2008.09.004

Bose, J., Parker, J. & McQuiston, F. (1985). *Design/data manual for closed-loop ground coupled heat pump systems*. Oklahoma State Univ for ASHRAE

Chen, J., Yang, L. & An, B. (2022). Unsteady analysis of the cold energy storage heat exchanger in a liquid air energy storage system. *Applied Energy*. 87(1), 16 – 27. https://doi.org/10.1016/j.apenergy.2009.04.038

Consejo de Ciencia y Tecnología del Estado de Querétaro (2002). *Uso Actual y Potencial del Suelo en los Municipios conurbados de Querétaro.* [PDF]. Disponible en: http://www.concyteq.edu.mx/concyteq//uploads/publicacionArchivo/2017-06-212.pdf

Eskilson, P. (1987). *Thermal analysis of heat extraction boreholes.* University of Lund. [PDF].

ISSN 2523-2881

Fundación de la Energía de la Comunidad de Madrid (2010). *Guía de la Energía Geotérmica. Dirección General de Industria, Energía y Minas*. Universidad Politécnica de Madrid, [PDF]. Disponible en: https://www.fenercom.com/wp-content/uploads/2008/01/Guia-de-la-Energia-Geotermica-fenercom-2008.pdf

Gong, Q., Yu, C., Wang, W. & Wang, Y. (2023). Experimental and numerical exploration on improved heat transfer by continuous spiral flow in shell of spiral wound corrugated tube heat exchanger, *International Journal of Thermal Sciences*, 191(), https://doi.org/10.1016/j.csite.2023.103483

Guo, L., Zhu, J. & Li, M. (2014). Research and prospect of enhanced heat transfer elements in inter-wall heat exchangers, Guangdong. *Chemical Industry*, 41, 101–107.

INEGI (2007). Marco Geo estadístico Municipal, conjunto de datos vectorial - edafológico, información topográfica digital. Disponible en: https://www.inegi.org.mx/app/biblioteca/ficha.html?upc=889463496731

INEGI (2021). *Aspectos geográficos: Querétaro.* [PDF]. Disponible en: https://www.inegi.org.mx/contenidos/app/areasgeograficas/resumen/resumen_22.pdf

Ingersoll, L. R., Adler, F. T., Plass, H. J. &Ingersoll, A. C. (1950). Theory of Earth Heat Exchangers for the Heat Pump. *Scientific Research Publishing Inc.* 56, 167-188. Available in: https://www.scirp.org/(S(351jmbntv-nsjt1aadkposzje))/reference/referencespapers.aspx?referenceid=682252

International Ground Source Heat Pump Association (2013). *Closed-loop/ground-source heat pump systems – Installation guide*. Oklahoma State University. Available in: https://geoconnectionsinc.com/resources/downloads/IGSHPA_Design_Installation_Standards.pdf

Kusuda, T. & Achenbach, P.R. (1965). *Earth temperature and thermal diffusivity at selected stations in the United States*. [PDF]. Available in: https://nvlpubs.nist.gov/nistpubs/Legacy/RPT/nbsreport8972.pdf

Lv, M., Yang, X. & Zhang, Y. (2018). Analysis of the current situation of heat exchangers and their classification and application. *Chemical Industry*. 47, 582–584.

Meteored (2023). *Histórico del clima en Querétaro.* Disponible en: https://www.meteored.mx/queretaro/historico

Mustafa, O. (2008). Ground-source heat pumps systems and applications. *Renewable and Sustainable Energy Reviews*, 12(2), 344-371. https://doi.org/10.1016/j.rser.2006.10.003

Philippe, M., Bernier, M., Marchio, D. & Lopez, S. (2011). A semi-analytical model for serpentine horizontal ground heat exchangers. *HVAC&R Research*, 17(6), 1044–1058. https://doi.org/10.1080/10789669.2011.607880
Rees, S. (2016). Advances in Ground Source Heat Pump Systems. https://doi.org/10.1016/C2014-0-03840-3

Rousseau, C., Comlan, F., Lamarche, L., Ouzzane, M. & Kajl, S. (2017). Modeling and experimental validation of a transient direct expansion geothermal heat exchanger. *Geothermics*, https://doi.org/10.1016/j.geothermics.2015.06.007

Sossa, V. & Sebastián, M. (2013). *Diseño e integración de energía geotérmica de baja entalpía aplicada a proyectos de construcción residencial*. Universidad de Chile. Disponible en: https://repositorio.uchile.cl/handle/2250/113790 The International Ground Source Heat Pump Association 2nd IGSHPA Research Track was hosted by IGSHPA Sweden and KTH. (2018 September 18-19). Stockholm, Sweden.

Triki, R., Hassene, D. & Baccar, M. (2021). Numerical investigation of heat treatment of an olive paste within a scraped surface heat exchanger equipped with helix screw. *Arabian Journal of Geosciences*, 14(2180), https://doi.org/10.1007/s12517-021-08535-9

Yang, H., Cui, P. & Fang, Z. (2009). Vertical-borehole ground-coupled heat pumps: a review of models and systems. *Applied Energy*, 87 (1), 16–27. https://doi.org/10.1016/j.apenergy.2009.04.038

ISSN 2523-2881

Zheng, G., Xiao, Q., Zhu, S., Wang, H., Geng, J., Zhao, S. & Huang, J. (2022). Analysis of heat transfer performance of ORC direct contact heat exchanger by GRA-VMD-LSSVM model using optimization. *Korean Journal of Chemical Engineering,* 39 () 1729–1743, https://doi.org/10.1007/s11814-022-1080-9

ISSN 2523-2881

[Title in Times New Roman and Bold No. 14 in English and Spanish]

Surname (IN UPPERCASE), Name 1st Author†*, Surname (IN UPPERCASE), Name 1st Coauthor, Surname (IN UPPERCASE), Name 2nd Coauthor and Surname (IN UPPERCASE), Name 3rd Coauthor

Institutional Affiliation of Author including Dependency (No.10 Times New Roman and Italic)

International Identification of Science - Technology and Innovation

ID 1st Author: (ORC ID - Researcher ID Thomson, arXiv Author ID - PubMed Author ID - Open ID) and CVU 1st author: (Scholar-PNPC or SNI-CONAHCYT) (No.10 Times New Roman)

ID 1st Coauthor: (ORC ID - Researcher ID Thomson, arXiv Author ID - PubMed Author ID - Open ID) and CVU 1st coauthor: (Scholar or SNI) (No.10 Times New Roman)

ID 2nd Coauthor: (ORC ID - Researcher ID Thomson, arXiv Author ID - PubMed Author ID - Open ID) and CVU 2nd coauthor: (Scholar or SNI) (No.10 Times New Roman)

ID 3rd Coauthor: (ORC ID - Researcher ID Thomson, arXiv Author ID - PubMed Author ID - Open ID) and CVU 3rd coauthor: (Scholar or SNI) (No.10 Times New Roman)

(Report Submission Date: Month, Day, and Year); Accepted (Insert date of Acceptance: Use Only ECORFAN)

Abstract (In English, 150-200 words)

Objectives
Methodology
Contribution

Abstract (In Spanish, 150-200 words)

Objectives
Methodology
Contribution

Keywords (In English)

Indicate 3 keywords in Times New Roman and Bold No. 10

Keywords (In Spanish)

Indicate 3 keywords in Times New Roman and Bold No. 10

Citation: Surname (IN UPPERCASE), Name 1st Author, Surname (IN UPPERCASE), Name 1st Coauthor, Surname (IN UPPERCASE), Name 2nd Coauthor and Surname (IN UPPERCASE), Name 3rd Coauthor. Paper Title. Journal Renewable Energy. Year 1-1: 1-11 [Times New Roman No.10]

* Correspondence to Author (example@example.org)
† Researcher contributing as first author.

Introduction

Text in Times New Roman No.12, single space.

General explanation of the subject and explain why it is important.

What is your added value with respect to other techniques?

Clearly focus each of its features

Clearly explain the problem to be solved and the central hypothesis.

Explanation of sections Article.

Development of headings and subheadings of the article with subsequent numbers

[Title No.12 in Times New Roman, single spaced and bold]

Products in development No.12 Times New Roman, single spaced.

Including graphs, figures and tables-Editable

In the article content any graphic, table and figure should be editable formats that can change size, type and number of letter, for the purposes of edition, these must be high quality, not pixelated and should be noticeable even reducing image scale.

[Indicating the title at the bottom with No.10 and Times New Roman Bold]

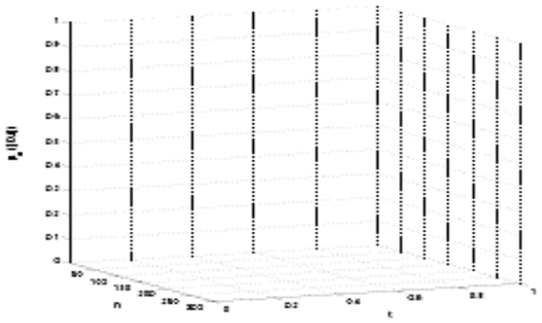

Graphic 1 Title and *Source (in italics)*

Should not be images-everything must be editable.

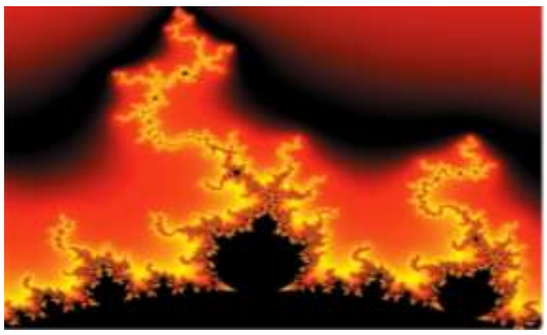

Figure 1 Title and *Source (in italics)*

Should not be images-everything must be editable.

Table 1 Title and *Source (in italics)*

Should not be images-everything must be editable.

Each article shall present separately in **3 folders**: a) Figures, b) Charts and c) Tables in .JPG format, indicating the number and sequential Bold Title.

For the use of equations, noted as follows:

$$Y_{ij} = \alpha + \sum_{h=1}^{r} \beta_h X_{hij} + u_j + e_{ij} \qquad (1)$$

Must be editable and number aligned on the right side.

Methodology

Develop give the meaning of the variables in linear writing and important is the comparison of the used criteria.

Results

The results shall be by section of the article.

Annexes

Tables and adequate sources

Thanks

Indicate if they were financed by any institution, University or company.

ISSN: 2523-2881

Conclusions

Explain clearly the results and possibilities of improvement.

References

Use APA system. Should not be numbered, nor with bullets, however if necessary numbering will be because reference or mention is made somewhere in the Article.

Use Roman Alphabet, all references you have used must be in the Roman Alphabet, even if you have quoted an Article, book in any of the official languages of the United Nations (English, French, German, Chinese, Russian, Portuguese, Italian, Spanish, Arabic), you must write the reference in Roman script and not in any of the official languages.

Technical Specifications

Each article must submit your dates into a Word document (.docx):

Journal Name
Article title
Abstract
Keywords
Article sections, for example:

1. Introduction
2. Description of the method
3. Analysis from the regression demand curve
4. Results
5. Thanks
6. Conclusions
7. References

Author Name (s)
Email Correspondence to Author
References

Intellectual Property Requirements for editing:

- Authentic Signature in Color of Originality Format Author and Coauthors
- Authentic Signature in Color of the Acceptance Format of Author and Coauthors
- Authentic Signature in Color of the Conflict of Interest Format of Author and Co-authors.

ISSN: 2523-2881

Reservation to Editorial Policy

Journal Renewable Energy reserves the right to make editorial changes required to adapt the Articles to the Editorial Policy of the Research Journal. Once the Article is accepted in its final version, the Research Journal will send the author the proofs for review. ECORFAN® will only accept the correction of errata and errors or omissions arising from the editing process of the Research Journal, reserving in full the copyrights and content dissemination. No deletions, substitutions or additions that alter the formation of the Article will be accepted.

Code of Ethics - Good Practices and Declaration of Solution to Editorial Conflicts

Declaration of Originality and unpublished character of the Article, of Authors, on the obtaining of data and interpretation of results, Acknowledgments, Conflict of interests, Assignment of rights and Distribution.

The ECORFAN-Mexico, S.C Management claims to Authors of Articles that its content must be original, unpublished and of Scientific, Technological and Innovation content to be submitted for evaluation.

The Authors signing the Article must be the same that have contributed to its conception, realization and development, as well as obtaining the data, interpreting the results, drafting and reviewing it. The Corresponding Author of the proposed Article will request the form that follows.

Article title:

- The sending of an Article to Journal Renewable Energy emanates the commitment of the author not to submit it simultaneously to the consideration of other series publications for it must complement the Format of Originality for its Article, unless it is rejected by the Arbitration Committee, it may be withdrawn.

- None of the data presented in this article has been plagiarized or invented. The original data are clearly distinguished from those already published. And it is known of the test in PLAGSCAN if a level of plagiarism is detected Positive will not proceed to arbitrate.

- References are cited on which the information contained in the Article is based, as well as theories and data from other previously published Articles.

- The authors sign the Format of Authorization for their Article to be disseminated by means that ECORFAN-Mexico, S.C. In its Holding Republic of Peru considers pertinent for disclosure and diffusion of its Article its Rights of Work.

- Consent has been obtained from those who have contributed unpublished data obtained through verbal or written communication, and such communication and Authorship are adequately identified.

- The Author and Co-Authors who sign this work have participated in its planning, design and execution, as well as in the interpretation of the results. They also critically reviewed the paper, approved its final version and agreed with its publication.

- No signature responsible for the work has been omitted and the criteria of Scientific Authorization are satisfied.

- The results of this Article have been interpreted objectively. Any results contrary to the point of view of those who sign are exposed and discussed in the Article.

Copyright and Access

The publication of this Article supposes the transfer of the copyright to ECORFAN-Mexico, SC in its Holding Republic of Peru for its Journal Renewable Energy, which reserves the right to distribute on the Web the published version of the Article and the making available of the Article in This format supposes for its Authors the fulfilment of what is established in the Law of Science and Technology of the United Mexican States, regarding the obligation to allow access to the results of Scientific Research.

Article Title:

Name and Surnames of the Contact Author and the Coauthors	Signature
1.	
2.	
3.	
4.	

Principles of Ethics and Declaration of Solution to Editorial Conflicts

Editor Responsibilities

The Publisher undertakes to guarantee the confidentiality of the evaluation process, it may not disclose to the Arbitrators the identity of the Authors, nor may it reveal the identity of the Arbitrators at any time.

The Editor assumes the responsibility to properly inform the Author of the stage of the editorial process in which the text is sent, as well as the resolutions of Double-Blind Review.

The Editor should evaluate manuscripts and their intellectual content without distinction of race, gender, sexual orientation, religious beliefs, ethnicity, nationality, or the political philosophy of the Authors.

The Editor and his editing team of ECORFAN® Holdings will not disclose any information about Articles submitted to anyone other than the corresponding Author.

The Editor should make fair and impartial decisions and ensure a fair Double-Blind Review.

Responsibilities of the Editorial Board

The description of the peer review processes is made known by the Editorial Board in order that the Authors know what the evaluation criteria are and will always be willing to justify any controversy in the evaluation process. In case of Plagiarism Detection to the Article the Committee notifies the Authors for Violation to the Right of Scientific, Technological and Innovation Authorization.

Responsibilities of the Arbitration Committee

The Arbitrators undertake to notify about any unethical conduct by the Authors and to indicate all the information that may be reason to reject the publication of the Articles. In addition, they must undertake to keep confidential information related to the Articles they evaluate.

Any manuscript received for your arbitration must be treated as confidential, should not be displayed or discussed with other experts, except with the permission of the Editor.

The Arbitrators must be conducted objectively, any personal criticism of the Author is inappropriate.

The Arbitrators must express their points of view with clarity and with valid arguments that contribute to the Scientific, Technological and Innovation of the Author.

The Arbitrators should not evaluate manuscripts in which they have conflicts of interest and have been notified to the Editor before submitting the Article for Double-Blind Review.

Responsibilities of the Authors

Authors must guarantee that their articles are the product of their original work and that the data has been obtained ethically.

Authors must ensure that they have not been previously published or that they are not considered in another serial publication.

Authors must strictly follow the rules for the publication of Defined Articles by the Editorial Board.

The authors have requested that the text in all its forms be an unethical editorial behavior and is unacceptable, consequently, any manuscript that incurs in plagiarism is eliminated and not considered for publication.

Authors should cite publications that have been influential in the nature of the Article submitted to arbitration.

Information services

Indexation - Bases and Repositories

LATINDEX (Scientific Journals of Latin America, Spain and Portugal)
EBSCO (Research Database - EBSCO Industries)
RESEARCH GATE (Germany)
GOOGLE SCHOLAR (Citation indices-Google)
MENDELEY (Bibliographic References Manager)
HISPANA (Information and Bibliographic Orientation-Spain)

Publishing Services

Citation and Index Identification H
Management of Originality Format and Authorization
Testing Article with PLAGSCAN
Article Evaluation
Certificate of Double-Blind Review
Article Edition
Web layout
Indexing and Repository
ArticleTranslation
Article Publication
Certificate of Article
Service Billing

Editorial Policy and Management

1047 La Raza Avenue -Santa Ana, Cusco-Peru. Phones: +52 1 55 6159 2296, +52 1 55 1260 0355, +52 1 55 6034 9181; Email: contact@ecorfan.org www.ecorfan.org

Journal Renewable Energy

2523 6881
ISSN 2523 - 6881

www.ecorfan.org